Traditional kriging versus modern Gaussian processes for large-scale mining data

Ryan B. Christianson*   Ryan M. Pollyea†   Robert B. Gramacy‡

December 16, 2022

Abstract

The canonical technique for nonlinear modeling of spatial/point-referenced data is known as kriging in geostatistics, and as Gaussian Process (GP) regression for surrogate modeling and statistical learning. This article reviews many similarities shared between kriging and GPs, but also highlights some important differences. One is that GPs impose a process that can be used to automate kernel/variogram inference, thus removing the human from the loop. The GP framework also suggests a probabilistically valid means of scaling to handle a large corpus of training data, i.e., an alternative to so-called ordinary kriging. Finally, recent GP implementations are tailored to make the most of modern computing architectures such as multi-core workstations and multi-node supercomputers. We argue that such distinctions are important even in classically geostatistical settings. To back that up, we present out-of-sample validation exercises using two, real, large-scale borehole data sets involved in the mining of gold and other minerals. We pit classic kriging against the modern GPs in several variations and conclude that the latter can more economical (fewer human and compute resources), more accurate and offer better uncertainty quantification. We go on to show how the fully generative modeling appraratus provided by GPs can gracefully accommodate left-censoring of small measurements, as commonly occurs in mining data and other borehole assays.

Keywords: ordinary kriging; Gaussian process regression; surrogate modeling; variogram; Vecchia approximation; multiple imputation

1   Introduction

The modern literature on spatial nonparametric regression (e.g., "kriging") traces its origins to the mining analytics of Danie Krige and Henri de Wijs and the subsequent work of Matheron (Matheron, 1971). Similar ideas were developed independently around the same time to aid the early analysis of computer simulation experiments, like those conducted in the study of nuclear weapons and energy, however (unclassified) publications did not appear until later (e.g., Sacks et al. (1989)). The spatial statistics community was responsible for much of the subsequent advances in methodology (e.g., Cressie (1993)), and software for kriging in use commercially (e.g., `LeapFrog`, `Vulcan`, `Surfer`, etc.) and academically (e.g., `GSLIB`) in mining today.

---

*Corresponding author: `rchristianson@vt.edu`, Department of Statistics, Virginia Tech

†Department of Geosciences, Virginia Tech 926 W. Campus Dr. Blacksburg, VA 24060

‡Department of Statistics, Virginia Tech, 250 Drillfield Dr. Blacksburg, VA 24061

More recently, researchers in geospatial statistics, surrogate modeling of computer experiments, and more broadly in statistical and machine learning communities, have pushed the boundaries of fidelity and computational tractability as modeling ambition and scale of data collection continue to grow, e.g., Gramacy (2020). These disparate literatures have converged around the nomenclature of Gaussian process (GP) regression as a generative framework for the kinds of data and procedures involved in kriging, but with a more cohesive and flexible approach to inference, approximation and automation based upon the likelihood, which is the foundation to modern statistcal learning.

Common geoscience applications for spatial smoothing and interpolation include ore-grade estimation and reservoir characterization/simulation; however, software tools utilized for such applications lag the state-of-the-art (as outlined above) by a decade or more. For example, obtaining fits requires expert human interaction with the software library and intuition in order to entertain alternatives of spanning anisotropies, neighborhood sizes of ordinary kriging in the face of large training data sets, and appropriate semivariogram forms modeling the decay of spatial correlation. Recent advances from the statistics and data analytics communities automate many of these time-consuming tasks, while offering substantial improvements in computational efficiency includeing the use of contemporary computing architectures such as multi-core workstations and clusters.

The main goal of this paper is to provide a review which focuses on the similararties and differences in these two frameworks. Ultimately we wish to advocate for the more modern, GP perspective via open-source libraries such as for R such as GPvecchia (Katzfuss et al., 2021) and laGP (Gramacy, 2016). These are just two of many which offer modern take on ordnary kriging, embodying advances in engineering and statistical learning: likelihood-based criteria offloaded to robust optimization libraries; human out-of-the-loop inference. Not only are they easy to use, but they are also hard to misuse.
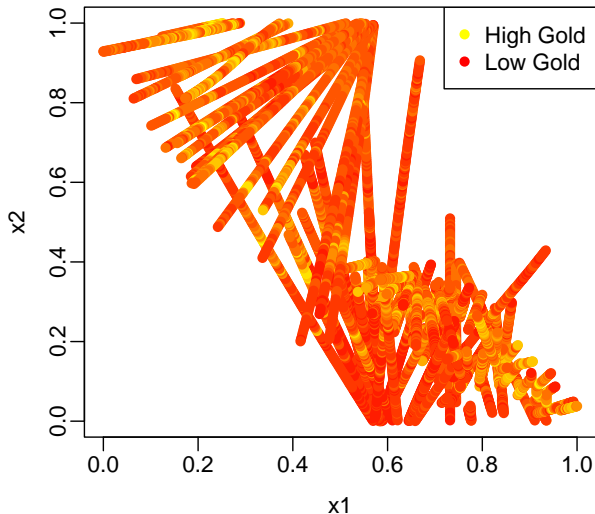

Figure 1: An example of borehole data as a 2d projection.

This narrative is backed up by empirical comparison. We consider two real data borehole-based mining examples with data records on gold and other minerals, over spatial and depth coordinates, sized in the hundreds of thousands. Figure 1 shows a 2d projection of a subset of the data described

in more detail in Section 4; note the long stretches of observations all in a line. These data exhibit many typical yet challenging features such as abrupt changes in dynamics, left-censoring of small values due to the sensitivity of the measurement instrument, and large measurement gaps in space. Using these data, we devise a cross-validation-based out-of-sample exercise which is careful to respect the borehole nature of data collection. The outcome of that exercise is evidence that modern GP-based methods are both more accurate, more hands-off, more economical (in terms of computing resources), and offer better uncertainty quantification than their kriging-based analogues. They also enable extensions which would be difficult to entertain without a fully probabilistic generative framework. As a showcase, we entertain a multiple imputation scheme to handle left censoring that involves only a few lines of code around library-based GP fitting and prediction subroutines.

The rest of the paper is outlined as follows. Section 2 contains a review of GP regression and kriging. Building on those, Section 3 contains the main, large-scale GP regression and kriging methods we compare using two real borehole ore data sets. Section 4 has cross validation results comparing those methods on both time and accuracy, including extensions to faciliate (without discarding) a large degree of left-censoring in one of the two data sets. Finally, Section 5 concludes with a discussion and ideas for future work.

2   GPs versus kriging

We begin by introducing Gaussian process (GP) regression with an eye toward connecting to kriging. At some level, they are the same thing. The biggest differences lie in vocabulary and inference for unknown quantities, which is coupled with the degree of automation/human intervention.

2.1   Gaussian Process Regression

Suppose we wish to model a function $f : \mathbb{R}^d \to \mathbb{R}$ with a limited number of noisy evaluations $y_i = f(x_i) + \epsilon_i$, for $i = 1, \ldots, N$. Let X_N be an $N \times d$ matrix formed with d-dimensional $x_i^\top$ in each of its rows. Similarly combine scalar outputs y_i into an N-vector Y_N. Throughout this paper, we privilege an input–output (x, y) notational scheme in keeping with the vast majority of the statistical learning literature on regression, nonparametric and nonlinear or otherwise. In many geospatial contexts (e.g., Banerjee, 2017), where f might be an environmental or geological process, it is common to use s_i for (spatial) input sites and $z_i = Z(s_i)$, among many alternatives, for the response. We think this unproductively biases thinking towards $d = 2$-dimensional point-referenced (latitude and longitude) data, whereas these methods can be applied much more widely than that. Machine learning (e.g., Rasmussen and Williams, 2006) and computer surrogate modeling (e.g., Gramacy, 2020) applications are typically in higher input dimension, and one of our goals in this paper is to introduce this way of thinking into the mining literature.

A common nonparametric model for such data is a Gaussian process (GP), which assumes that outputs Y_N follow a multivariate normal (MVN) distribution. Inputs X_N are primarily involved in the specification of the MVN covariance $\Sigma_N \equiv \Sigma(X_N, X_N)$ with a form for $\Sigma(\cdot, \cdot)$ that inverts Euclidean distances between its arguments. For example,

$$Y_N \sim \mathcal{N}_N(0, \Sigma_N), \quad \text{where} \quad \Sigma_N^{ij} \quad \text{follows} \quad S\left(\frac{1}{\text{Dist}(x_i, x_j)}\right) \quad \text{for some decreasing } S. \quad (1)$$

3

In Eq. (1) we are being deliberately imprecise about the form of Σ_N, a topic we shall detail shortly in Section 2.2. For now, simply suppose correlation in outputs decays as a function of distance in inputs: $\mathbb{C}\mathrm{orr}(y_i, y_j) < \mathbb{C}\mathrm{orr}(y_i, y_k)$ if x_i is "closer" to x_k than it is to x_j. We are also using a zero mean specification, so that all of the modeling "action" is in the covariance. Extensions abound.

Although a Bayesian interpretation is not essential in characterizing GP regression, Eq. (1) can be said to specify a prior over (noisy evaluations of) functions like f, abstracting as $Y_N \sim \mathrm{GP}$. Choices for the mean (0) and variance (Σ) determine the modeling properties of f like its smoothness and wiggliness. We shall largely leave those properties to our references, except as relevant to particular choices for $\Sigma(\cdot, \cdot)$, again in Section 2.2. Then, if N' new locations $\mathcal{X}$ come along where we do not yet have observations, $Y(\mathcal{X})$, we can summarize our understanding for those in light of the (training) data we do have – a predictive distribution – through the lens of posterior conditioning: $Y(\mathcal{X}) \mid Y_N$. First, extend the GP prior to cover $Y(\mathcal{X})$ jointly with Y_N:

$$\begin{bmatrix} Y_N \\ Y(\mathcal{X}) \end{bmatrix} \sim \mathcal{N}_{N+N'} \left(\begin{bmatrix} 0 \\ 0 \end{bmatrix}, \begin{bmatrix} \Sigma_N & \Sigma(X_N, \mathcal{X}) \\ \Sigma(\mathcal{X}, X_N) & \Sigma(\mathcal{X}, \mathcal{X}) \end{bmatrix} \right).$$

In so doing, we may leverage that $Y(\mathcal{X})$ values are more highly correlated with Y_N values whose X_N entries are close to $\mathcal{X}$ ones by applying standard MVN conditioning rules, such as those found in Kalpić and Hlupić (2011), $Y(\mathcal{X}) \mid Y_N \sim \mathcal{N}_{N'}(\mu_N(\mathcal{X}), \Sigma_N(\mathcal{X}))$ where

$$\mu_N(\mathcal{X}) = \Sigma(\mathcal{X}, X_N)\Sigma_N^{-1} Y_N \qquad (2)$$
$$\Sigma_N(\mathcal{X}) = \Sigma(\mathcal{X}, \mathcal{X}) - \Sigma(\mathcal{X}, X_N)\Sigma_N^{-1}\Sigma(X_N, \mathcal{X}).$$

Note that $\Sigma_N(\mathcal{X})$ and $\Sigma(\mathcal{X}, \mathcal{X})$ are $N' \times N'$ matrices; the N subscript serves as a reminder of conditioning on Y_N. Observe that $\mu_N(\mathcal{X})$ is a (high dimensional) linear projection of those Y_N values, where the "weights" involved are inversely proportional to the distance between their X_N values and those of $\mathcal{X}$. Such conditioning identities apply for any MVN, based on a GP prior or otherwise. The special thing about the regression context is the (inverse) distance-based dynamics manifest as $\mathcal{O}(N)$ weights in each row of $\Sigma(\mathcal{X}, X_N)$, and $\mathcal{O}(N^2)$ in Σ_N, involved in the projection, rather than the usual $\mathcal{O}(d)$ or $\mathcal{O}(d^2)$ weights in, say, an ordinary linear regression. That higher-dimensional linear projection, $\mu_N(\mathcal{X})$, has properties that transcend the Bayesian interpretation. For example, under certain conditions it is a best linear unbiased predictor (BLUP). Although much of modern statistical learning now understands Eq. (2) in a wider, primarily Bayesian GP context, they are identical to the so-called *kriging equations* (Matheron, 1963), which have been instrumental in geospatial/mining analysis for more than half a century.

To illustrate Eq. (2) consider $f(x) = 2 + 2\sin(4\pi x)$, observed at $N = 20$ x_i-values uniform in $[0, 1]$ as $y_i = f(x_i) + \varepsilon_i$, where $\varepsilon_i \overset{\text{iid}}{\sim} \mathcal{N}(0, 0.1)$. While GP regression is usually applied in higher dimension, such as 2d and beyond, the 1d setting is convenient for visualization. These twenty (x_i, y_i) pairs comprise of our "training data" (Y_N, X_N). Now, suppose we had a dense testing grid of $N' = 1000$ predictive locations $\mathcal{X}$ covering $[0, 1]$. Applying Eq. (2) would provide us with an N' vector of predictive means $\mu_N(\mathcal{X})$ and an $N' \times N'$ matrix of predictive covariances $\Sigma_N(\mathcal{X})$ summarizing our regression of y onto x. Variances $\sigma_N^2(\mathcal{X})$ along the diagonal of $\Sigma_N(\mathcal{X})$ could be used to build error-bars describing a predictive interval (PI) as roughly $\mu_N \pm 2\sigma_N$ for 95% coverage.

These quantities are shown for one example of such data in Figure 2. Noisy data evaluations (solid dots) dance around the true unknown function f (black line); our prediction(s) μ_N and PIs
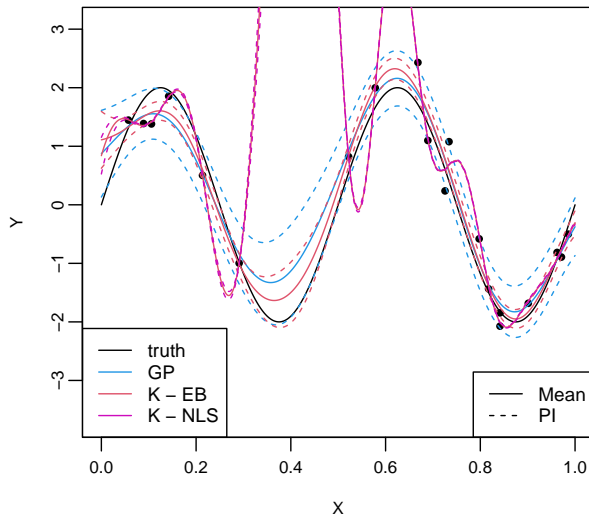
Figure 2: A 1d example function in black with dots being the observed locations. The GP prediction is in blue with dashed lines being the 90% predictive interval (PI). Kriging predictions are shown in red and magenta with EB and NLS referring to different variography techniques.

in (blue/red lines, dashed respectively) in two variations (labeled "GP" and "Kriging") accurately distill the essence of the input-output relationship. All of this is modulo a fortuitous choice for $\Sigma(\cdot, \cdot)$ which we have yet to detail. Its specification, and method of inference or unknown quantities, comprises the wedge between modern GPs (red in the figure) and traditional kriging (blue).

2.2 Modeling

The discussion above hinges on a choice of $\Sigma(\cdot, \cdot)$, or S in Eq. (1). S was merely used as a notational device to delay discussion until this moment; we shall not use S going forward. Yet, that Eq. (1) formulation is attractive because it abstracts all modeling details down to this "one" choice. "One" is in quotes because $\mathcal{O}(N^2)$ quantities, one for each pair of N data elements (x_i, y_i), are actually constrained by the covariance structure. This vast number of potentially tunable quantities, more even than N, is why one refers to GPs as nonparametric. But of course, it's neither practical nor valid to allow oneself such unbridled freedoms. For example, we must choose $\Sigma(\cdot, \cdot)$ so that Σ_N is finite and positive definite for use as an MVN covariance.

An inverse-distance-based covariance is conventional as an intuitive spatial modeling device. However, this is not a requirement and may not be ideal in all situations, e.g., when modeling periodic effects. We may wish to allow flexibility in how distances are measured, in what coordinates and with what decay in inversion, and to control how such choices relate signal to noise. Such considerations lead to frameworks for choices of $\Sigma(\cdot, \cdot)$ whose tunable quantities, sometimes called *hyperparameters* to acknowledge a nonparametric modeling apparatus, can be learned from data.

For example, if the range of the responses Y_N is unknown *a priori* we might wish to design $\Sigma(\cdot, \cdot)$ to include a scale hyperparameter, say τ^2. If Y_N is noisy and/or contains measurement error, we may wish to encode it as part signal, and part noise. Sometimes this is governed by a so-called *nugget* hyperparameter, which we shall denote as g. We caution that the role of GP nugget is inspired by,

5

but is subtly different from, a parameter of the same name in the geostatistics/kriging literature. More in Section 2.4. We may wish to control the smoothness and rate of decay of correlation of the signal in terms of (inverse) distance, and thereby the smoothness and other properties of the underlying response surface. This may be accomplished through selection of a so-called *kernel* function $k_\theta(x_i, x_j) : \mathbb{R}^d \to [0,1]$ whose hyperparameter θ can be used to describe the rate of radial decay from $k_\theta(x_i, x_j) = 1$ for $x_i = x_j$ down to zero as x_j moves away from x_i in an isotropic modeling context. Kernels k may also re-scale and/or rotate the space for anisotropic effects.

One way to put these elements together is

$$\Sigma(x_i, x_j) = \tau^2(k_\theta(x_i, x_j) + g\delta_{ij}) \quad \text{so that} \quad \Sigma_N = \tau^2(K_N + g\mathbb{I}_N). \tag{3}$$

Above, δ_{ij} is the Kronecker delta function returning 1 when the index $i = j$, i.e., when the same training data element appears in both arguments, and zero otherwise, and $K_N \equiv k_\theta(X_N, X_N)$ applying k elementwise as $K_N^{ij} = k_\theta(x_i, x_j)$. Observe that the diagonal of Σ_N is $\tau^2(1+g)$ and all off-diagonal entries are less than or equal to τ^2, and strictly less than for all $x_i \neq x_j$. This discontinuity between diagonal and off-diagonal, as long as $g > 0$, leads to smoothing of the predictive surface when following Eq. (2). Otherwise, when $g = 0$ the surface interpolates. Again, this is a little different than the typical geostatistics formulation as explained later in Section 2.4.

Choices for distance-based kernels k preserving positive definiteness and targeting certain other properties abound. See, e.g., Abrahamsen (1997) or Wendland (2004). The two that are most widely used are the power exponential and the Matérn. These are provided below in an isotropic setting, i.e., with radial decay as a function of distance.

$$k_\theta^P(x_i, x_j) = \exp\left\{-\frac{||x_i - x_j||^p}{\theta}\right\}$$

$$k_\theta^M(x_i, x_j) = \frac{2^{1-\nu}}{\Gamma(\nu)}\left(||x_i - x_j||\sqrt{\frac{2\nu}{\theta}}\right)^\nu \mathcal{K}_\nu\left(||x_i - x_j||\sqrt{\frac{2\nu}{\theta}}\right) \tag{4}$$

In both cases above the hyperparameter θ appears in the denominator, scaling (squared or square root) Euclidean distances between x_i and x_j, and is thus sometimes called the *characteristic length-scale*. Both have additional hyperparmeters, p and ν, respectively, which must be positive and which our notation does not include in θ because they are usually specified, rather than inferred with more discussion provided in Section 5. These control the of the resulting response surface. When $p = 2$ the power exponential produces infinitely smooth (mean-square differentiable) realizations, and sometimes this special case is called the Gaussian kernel,[1] which we denote as k_θ^G. When $p \neq 2$, the surface is nowhere differentiable. While sometimes such pathological non-smoothness is a reasonable assumption – and in spite of this the predictive surfaces (2) often look smooth – there are better mechanisms for relaxing unreasonable (infinite) smoothness.

Many of the choices in our references above offer higher fidelity control over smoothness (beyond none and infinite). Of those, the Matérn has percolated into the canonical position thanks largely to persuasive technical arguments from Stein (1999). The parameter ν controls this aspect, with higher values leading to greater smoothness, yielding surfaces which are $\lceil \nu \rceil - 1$ mean-square differentiable.

---

[1] *Gaussian* here refers to the expression resembling the density of a Gaussian distribution; it has nothing to do with making a Gaussian assumption, or its use in GP. Such kernels are used in a variety of other contexts.

Ultimately when $\nu \to \infty$ the Gaussian kernel is recovered as a special case. However, the modified Bessel function $\mathcal{K}_\nu$ can be difficult to work with computationally. Specific settings with $\nu \in \left\{ \frac{3}{2}, \frac{5}{2} \right\}$ have algebraic closed forms (no Bessel functions) which yield degree one and two differentiability, with the latter being most often applied in practice because most interesting dynamics result from at least twice (but not infinitely) differentiable processes.

Both the (isotropic) power exponential/Gaussian and Matérn are *stationary* kernels because they are defined only in terms of displacement $||x_i - x_j||$, so the resulting response surface would have identical dynamics throughout the entire input space. Nonstationary modeling is also possible, but is a lot more difficult in general. See, e.g., Sauer et al. (2021), and further discussion in Section 3.1. However, one can still capture nontrivial dynamics with stationary kernels, for example by deploying several of them simultaneously: sums, products, convolutions (and more) of valid kernels for GP regression (i.e., are positive definite) are also valid. For details, see e.g., Rasmussen and Williams (2006, , Section 4.2.4) or Gramacy (2020, , Section 5.3.3). One of the most common applications of this result is to extend to axis-aligned anisotropy by taking a product of kernels applied univariately in each coordinate direction: $k_\theta(x_i, x_j) = \prod_{k=1}^{d} k_{\theta_k}(x_{ik}, x_{jk})$, abusing the notation somewhat. This can be done with any kernel. Notice here we are introducing a d-dimensional lengthscale parameter $\theta = (\theta_1, \ldots, \theta_d)$, controlling the rate of spatial correlation differentially in each coordinate direction. For the Gaussian kernel, the result is identical to

$$k_\theta^G(x_i, x_j) = \exp \left\{ - \sum_{k=1}^{d} \frac{(x_{ik} - x_{jk})^2}{\theta_k} \right\}, \tag{5}$$

which is sometimes called the *separable* Gaussian kernel or the ARD Gaussian kernel. ARD stands for *automatic relevance determination* (Liu et al., 2020), borrowing terminology from early neural networks literature. The idea is that the data can inform on longer lengthscales (less relevant) or shorter ones (more relevant) for each input variable separately. ARD/separable Matérn kernels are also common, but their expression(s) are less tidy so we do not include it here. For more discussion, consult Rasmussen and Williams (2006) or Gramacy (2020).

There is a one-to-one relationship between vectorized lengthscale in the ARD kernel formulation and with re-scaling inputs X_N, say as a pre-processing step. Rather than scaling each input differently, one can extend this idea to rotations and projections to accommodate less rigid anisotropy either as preprocessing or as a hyperparameterized kernel formulation. For an example of a pre-processing approach see Wycoff et al. (2021) and references therein; for learning rotations and projects *within* a kernel see Gramacy and Lian (2012). We find that such high-powered approaches are overkill for most applications, including the mining ones discussed later.

2.3 Inference

The models above have tunable quantities, or hyperparameters, that could be set by hand but would ideally be learned from data. We restrict our focus to those which we introduced for $\Sigma(\cdot, \cdot)$, particularly $\phi \equiv (\tau^2, g, \theta)$ with the latter usually vectorized in an ARD setting, but there could potentially be additional quantities which must be estimated from data. There are many criteria and algorithms across several literatures devoted to such "fitting" enterprises (e.g., Diggle and Ribeiro, 2007). Yet there is a remarkable confluence in modern statistical learning practice when

it comes to the near universality of likelihood-based methods when distributional assumptions are being made (like the MVN in Eq. (1)). The reason is that no additional criteria need be introduced to commence with learning. One may choose to impose additional assumptions, like priors on aspects of ϕ for a Bayesian approach (Banerjee, 2017, which is still likelihood-based), or not – simply maximize the likelihood. This is the approach we present here because it is tidy and fast.

Eq. (1) depicts how observations/outputs (like Y_N), are distributed in relation to inputs (like X_N) and parameters or other structure (like $\Sigma(\cdot, \cdot)$ via hyperhaparameters ϕ and kernels k). The *likelihood* simply re-frames the density of that distribution, which assigns positive real values to Y_N as a function of parameters (or hyperparameters ϕ, say), the other way around: providing positive reals for ϕ given Y_N. Once in that context, it makes sense to seek out the parameterization that makes the observed Y_N most likely, i.e., that maximizes the likelihood. There are two benefits to this approach. One is that it reduces a statistical inference question to an optimization one without introducing auxiliary criteria. The other is that the solution to this optimization, the so-called maximum likelihood estimator (MLE), has special properties that can be used to quantify uncertainty. For a review of likelihood-based inference, see Casella and Berger (2001).

By inspecting the MVN density (Kalpić and Hlupić, 2011), using a mean of zero and covariance Σ_N, one may obtain the following expressions for the likelihood and its logarithm.

$$L(\phi; Y_N) = (2\pi)^{-\frac{N}{2}} |\Sigma_N|^{-\frac{1}{2}} \exp\left\{-\frac{1}{2} Y_N^\top \Sigma_N^{-1} Y_N\right\} \tag{6}$$

$$\ell(\phi; Y_N) = \log(L(\phi; Y_N)) = -\frac{N}{2}\log 2\pi - \frac{1}{2}\log|\Sigma_N| - \frac{1}{2}Y_N^\top \Sigma_N^{-1} Y_N$$

Recall from Eq. (3) that the parameters ϕ are embedded in $\Sigma_N = \tau^2(K_N + g\mathbb{I}_N)$ via K_N which is built through pairwise application of $k_\theta(\cdot, \cdot)$. Technically, this is a *marginal likelihood* since it tacitly defines both prior (which is integrated out) and observational variability. But this distinction is not important for our discussion. The curious reader is referred to Section 5.3.2 of Gramacy (2020). The log likelihood helps with maximization, easing differentiation but preserving critical points.

Consider τ^2 first. Observe that

$$\ell(\phi; Y_N) = c_1 - \frac{N}{2}\log\tau^2 + \frac{N}{2\tau^2}Y_N^\top \Sigma_N^{-1} Y_N$$

where $c_1 = -\frac{N}{2}\log 2\pi - \frac{1}{2}\log|K_N + g\mathbb{I}_N|$ is constant with respect to τ^2. Differentiating with respect to τ^2, setting to zero and solving, is straightforward.

$$0 \stackrel{\text{set}}{=} \frac{d\ell(\phi; Y_N)}{d\tau^2} = -\frac{N}{2\tau^2} + \frac{1}{2(\tau^2)^2}Y_N^\top(K_N + g\mathbb{I}_N)^{-1}Y_N^\top \quad\rightarrow\quad \hat{\tau}^2 = \frac{Y_N^\top(K_N + g\mathbb{I}_N)^{-1}Y_N}{N} \tag{7}$$

If we then plug $\hat{\tau}^2$ back into $\ell(\phi; Y_N)$ we get what is known as a concentrated, or profile log likelihood:

$$\ell(\theta, g; Y_N) = \ell(\phi; Y_N)\big|_{\tau^2=\hat{\tau}^2} = c_2 - \frac{N}{2}\log Y_N(K_N + g\mathbb{I}_N)^{-1} - \frac{1}{2}\log|K_N + g\mathbb{I}_N|$$

where c_2 is not a function of θ or g. Differentiation here is more challenging because the parameters are buried within matrix inverses and determinants. But it is still doable. See, e.g., Eq. (5.9) in
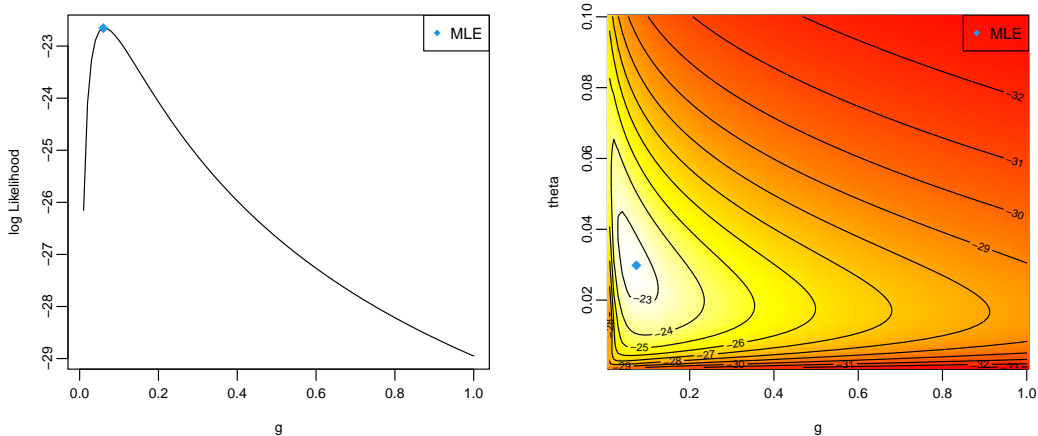
Figure 3: Log likelihood surfaces for the function in Figure 2. Left: Surface for g, holding τ^2 and θ constant at their MLE values. Right: Surface for g and θ, holding τ^2 at its MLE value.

Gramacy (2020). We have

$$\frac{d\ell(\theta, g; Y_N)}{dg} = \frac{N}{2} \frac{Y_N^\top ((K_N + g\mathbb{I}_N)^{-1})^2 Y_N}{Y_N^\top (K_N + g\mathbb{I}_N)^{-1} Y_N} - \frac{1}{2} \text{tr}((K_N + g\mathbb{I}_N)^{-1}) \tag{8}$$

$$\frac{d\ell(\theta, g; Y_N)}{d\theta} = \frac{N}{2} \frac{Y_N^\top K_N^{-1} K_N' (K_N + g\mathbb{I}_N)^{-1} Y_N}{Y_N^\top (K_N + g\mathbb{I}_N)^{-1} Y_N} - \frac{1}{2} \text{tr}((K_N + g\mathbb{I}_N)^{-1} K_N'),$$

where $K_N' = \frac{dK_N}{d\theta}$. The former is actually a special case of the latter, taking instead θ as g, since $\frac{d(K_N + g\mathbb{I}_N)}{dg} = \mathbb{I}_N$. When θ are lengthscales in k_θ, K_N' is formed of $(K_N')^{ij} = dk_\theta(x_i, x_j)/d\theta$, i.e., with component-wise derivatives of the kernel, say Gaussian or Matérn, with respect to θ. When θ is vectorized, we may instead calculate $\partial\ell(\theta, g; Y_N)/\partial\theta_k$, forming a gradient for $k = 1, \ldots, d$.

The next step is to set these derivatives to zero, either simultaneously or separately, and solve. However, no algebraic solution is known. Library-based numerical optimization, such as BFGS (Byrd et al., 1995) provided in R's `optim` function, can be used to find MLEs $\hat{g}$ and $\hat{\theta}$. Convergence is usually both robust and fast, even in high dimension d, when gradients (8) are provided since the underlying $\ell(\theta, g; Y_N)$ surface is almost always convex. To illustrate, Figure 3 shows $\ell(\theta, g; Y_N)$ using data associated with Figure 2. The left panel varies g conditional on a setting of θ, whereas the right panel varies both. In both cases, $\hat{\tau}^2$ has been concentrated out. Note that raw (un-logged) likelihood surfaces are even more peaked than these figures present. Regardless, it is easy to eyeball the MLE. R's `optim` is able to find $\hat{g}$ and $\hat{\theta}$, shown as blue diamonds in both panels in seventy-nine iterations. Looking back at Figure 2, the blue curves correspond to predictive surfaces uses these MLE hyperparamters. The red and magenta curves are detailed in the next subsection.

2.4   Kriging and Variography

The main difference between classical kriging and the GP presentation above regards inference for unknown quantities and, in the case of the latter, a more up-front and highly-leveraged distributional assumption (Gaussian) for the response. Both use Eq. (2) to form predictions and quantify

uncertainty. In geostatistics, these are known as the "kriging equations," even when other aspects historically associated with kriging are not faithfully replicated. Classical kriging focuses on lower input dimension – particularly $d \in \{2, 3\}$ in spatial contexts – and as such prefers isotropic modeling after a suitable transformation of spatial inputs. *Variography* is used to select the kernel and its hyperparameters, rather than the likelihood. This has advantages and disadvantages. Many of the advantages are related to the historically larger training data sets encountered in spatial problems, although that gap is narrowing in wider statistical learning and computer experiments contexts. More on this in Section 3, wherein further distinctions arise. The main disadvantage is that input pre-processing and variogram inspection are inherently hands-on, human driven enterprises, albeit ones enhanced by computational tools. Other differences are more superficial, like naming, symbol choice and applications of hyperparameters within variography.

The *semivariogram*, or half the *variogram*, denoted as $\gamma(h)$, is the variance of two output y-values that are distance h apart in the input x-space: $\gamma(h) = \frac{1}{2}\text{Var}(Y(x + h) - Y(x))$. Implicit in this definition is an assumption of intrinsic stationarity, implying that $\mathbb{E}[Y(x + h) - Y(x)] = 0$, or that the covariance between two y values depends not on position but on relative distance notated by the displacement h between them. If h is calculated using Euclidean distance, intrinsic stationarity implies isotropy. When this is a limitation to effective spatial modeling, one may prescale or rotate the coordinate system. This is often based on expert-judgment of the prevailing variabilities within the input domain, like the direction of an ore body within the geologic topology. As mentioned earlier, a modern GP approach would deploy separable lengthscales (5), or more flexibly parameterized rotations and scales that are learned jointly with other unknowns.
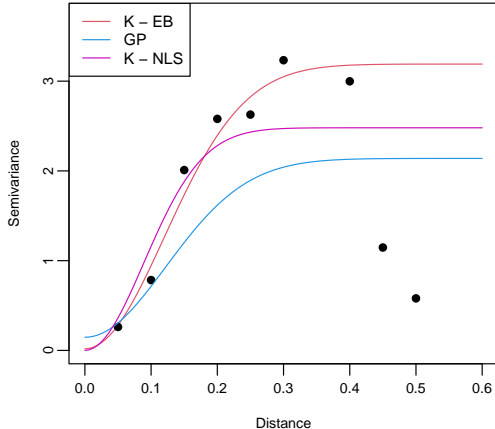
The semivariogram is a theoretical/population construct that would be hard to specify *a priori* even with expert knowledge, but simple to observe empirically given data. One estimate of an *empirical semivariogram* could be obtained by binning the data by distance and calculating sample covariances within those bins. Let $N(h_k) = \{(x_i, x_j) : ||x_i - x_j|| \in I_k\}$ where $I_1 = [0, h_1], I_2 = (h_1, h_2], \ldots, I_k = (h_{k-1}, h_k]$ denote a neighborhood structure striated by bands of distance $0, h_1, \ldots, h_k$. Then estimate

$$\hat{\gamma}(h) = \frac{1}{2|N(h)|} \sum_{(x_i, x_j) \in N(h)} (y_i - y_j)^2. \tag{9}$$

As defined continuously for any h, $\hat{\gamma}(h)$ is a step function. However it is customarily visualized discretely as a scatter plot with $(h_i + h_{i+1})/2$ as the x-axis coordinate. The left panel of Figure 4 shows these as dots for the 1d problem introduced in Figure 2 using a bin size $(h_{i+1} - h_i)$ of 0.05.

One can then match these empirical observations of spatial covariance with a parameterized form for the population semivariogram. Here, similar constructs are used to model spatial dependence as the kernels introduced earlier (4). Let $\gamma(0) = 0$ and for $h > 0$, power exponential and Matérn model semivariograms are often written as

$$\gamma_\theta^P(h) = \tau_k^2 + \sigma^2 \left(1 - \exp\left\{ -\left(\frac{h}{R} \right)^p \right\} \right)$$

$$\gamma_\theta^M(h) = \tau_k^2 + \sigma^2 \left(1 - \frac{2^{1-\nu}}{\Gamma(\nu)} \left(h\sqrt{\frac{2\nu}{R}} \right)^\nu \mathcal{K}_\nu \left(h\sqrt{\frac{2\nu}{R}} \right) \right). \tag{10}$$

Figure 4: A Gaussian kernel/semivariogram fit to the function in Figure 2. "EB" denotes a semivariogram fit by hand, whereas "NLS" uses non-linear least squares; "GP" derives the semivariogram from an MLE hyperparameterization. The table compares hyperparameter estimates.

Semivariogram parameters are known as *nugget* (τ_k^2),[2] *partial sill* (σ^2), and *range* (R).

Taking $\gamma(0) = 0$ is a contentious choice outside of the geospatial modeling literature. It implies that there is no intrinsic variance in measurements. In part this is because such measurements are inherently unrepeatable in certain contexts; you cannot dig a borehole in the same place twice. But if you could, it stands to reason that you would get different measurements for such *replicates* for all sorts of reasons, e.g., even without operator error the drill bit might interact with the surface and ore body differently the second time. Primordial process producing the ore body are subject to uncertainties that are best characterized as random variables even if the process is not inherently stochastic. Thus, it is acknowledged that there will be small-scale variability between *nearby* observations that are best described by noise. This noise, at all distances $h = \epsilon > 0$, is what is parameterized by the nugget τ_k^2. The distinction with the GP nugget g, which characterizes the noise as $\tau^2 g$ at $h = 0$, is thus subtle. Choosing $\gamma(0) = 0$ has an impact on the kriging equations (2), leading to discontinuities at the training data locations, where an otherwise smooth predictive surface would be pocked with spikes of "interpolation." We do not show these in the red curve by deliberately omitting X_N values from our predictive grid $\mathcal{X}$ for Figure 2 for aesthetic reasons.

Kriging-versus-GP distinctions between the other two kernel parameters are more superficial. The partial sill σ^2 controls the maximum covariance as $h \rightarrow \infty$. This has a 1:1 correspondence with the τ^2 from earlier. Sometimes the *sill* parameter, $\tau_k^2 + \sigma^2$, is preferred by geostatisticians instead. The range R controls the distance between maximum and minimum covariance, and plays an identical role as the square root lengthscale: $R = \sqrt{\theta}$. It is not uncommon to instead specify a decay parameter $\phi = 1/R$, and such inversions are common in the GP literature as well.

Each setting of these parameters could be used to overlay a curve onto the left panel of Figure 4. For example, using the MLE hyparameters from our earlier GP analysis yields the curve in blue. Alternatively, one could automate a search for the "best fitting" variogram parameteriza-

---

[2]A subscript k is not standard; we added it to distinguish with the GP scale τ^2.

tion with a generalized/nonlinear (possibly weighted) least-squares (NLS) criterion (Cressie, 1985). This corresponds to the magenta curve. Observe that neither of these result in a terrific fit to the semivariogram "data." An outlying pair of dots near $h = 0.5$ drags these variograms down, sacrificing fit for smaller pairwise distances. One reason these are outlying may be that we have many fewer long-distance pairs in the data than short distance ones. A common remedy would be to downweight or altogether ignore these when fitting the variogram parameters, focusing only on the short distance readings. We refer to one such fit as the "eyeball" (or EB) variogram in the figure, although in practice NLS may similarly be deployed. This can lead to more accurate predictions out-of-sample, as we demonstrate momentarily. However it has the downside of introducing non-statistical (e.g., NLS) and non-metric (determination of outlying semivariogram estimates) criteria which diminishes reproducibility and automation, and incurs the expense of human expert intervention. This enterprise is also sensitive to other choices such as bin size $h_{i+1} - h_i$ and a choice of maximum distance to calculate the empirical variogram. We chose $h_{\max} = 0.5$ for Figure 4, but could have gone out to $h_{\max} = 1$, producing a much "noisier" empirical semivariogram.

Figure 4 details hyperparameter estimates for each of the three techniques. Lengthscale and range settings exhibit high agreement. For scale/partial sill, NLS and GP MLE values are "drawn down" by the noisier higher distance bins relative to our EB alternative which ignored those values. The nugget is where things start to substantially diverge: $\tau^2 g \gg \tau_k^2$ means our GP-MLE estimates more noise/less signal than the kriging alternatives (EB and NLS). Notice that EB and NLS nuggets are on different orders of magnitude. The tiny NLS τ_k^2 may be attributed to a lack of small distance pairs, and consequently the optimizer converged at the boundary of our search space for that parameter: 10^{-4}, meaning very high signal/low noise. Although this seems innocuous when it comes to the corresponding semivariograms on the left in the figure, the implications out-of-sample are severe. This is foreshadowed in Figure 2, and evaluated empirically next.

2.5 Out of Sample Validation

In Figure 2 the EB kriging fit (solid-red) is visually similar to the GP-MLE fit (solid-blue) except perhaps near $x = 0.4$. This is noteworthy in light of the disparate parameterization and semivariograms in Figure 4, and in particular the human intervention required to ignore outlying values in favor of short distances. Qualitatively, the red curve may be more accurate compared to the truth (black), but closer inspection reveals a more pernicious concern despite apparent higher accuracy: poor uncertainty quantification. The red 90% PI (error-bars) cover only about half of the training data locations, suggesting that nominal coverage has not been achieved. In contrast, the blue (GP-MLE) error-bars cover many more of the data points.

There are many ways to be more precise about out-of-sample prediction accuracy. Consider a testing set comprised of a grid of $\mathcal{X}$-values of size N' with true values $y(\mathcal{X})$. Given predictions from a kriging/GP fit (2), notated generically as $\mu(\mathcal{X})$, the *proper scoring rule* (Gneiting and Raftery, 2007) is root mean square error (RMSE).

$$\text{RMSE}(y(\mathcal{X}), \mu(\mathcal{X})) = \sqrt{\frac{1}{N'} \sum_{i=1}^{N'} (y_i(x_i) - \mu_i(x_i))^2} \tag{11}$$

1d	GP	K-EB	K-NLS
RMSE	0.14	0.084	23.11
score$_\text{f}$	869	-4161	-1255140

Table 1: Out-of-sample RMSE and score for GP and kriging on the 1d toy problem.

Lower RMSE is better. The first row of the left panel of Table 1 shows that the mean predictions for kriging via EB are indeed more accurate than via MLE.

If one also has covariances $\Sigma(\mathcal{X})$, or just variances $\sigma^2(\mathcal{X}) = \text{diag}(\Sigma(\mathcal{X}))$, associated with predictions, the proper scoring rule is more complex as accuracy must be normalized by uncertainty:

$$\text{score}_\text{f}(Y(\mathcal{X}), \mu(\mathcal{X}), \Sigma(\mathcal{X})) = -\log(|\Sigma(\mathcal{X})|) - (Y(\mathcal{X}) - \mu(\mathcal{X}))^\top \Sigma(\mathcal{X})^{-1}(Y(\mathcal{X}) - \mu(\mathcal{X})) \quad (12)$$

$$\text{score}_\text{p}(Y(\mathcal{X}), \mu(\mathcal{X}), \sigma^2(\mathcal{X})) = -\sum_{i=1}^{N'} \log(\sigma_i^2) - \sum_{i=1}^{N'} \left(\frac{(Y_i(x_i) - \mu_i(x_i))^2}{\sigma_i^2} \right).$$

In these equations an upper-case $Y(\mathcal{X})$ is used to convey that a comparison is being made to noisy sample of Y-values following the data-generating mechanism, Observe that score based on full covariance (score$_\text{f}$) is the out-of-sample analog of the log likelihood (6), i.e., within an additive and multiplicative constant of criteria deplored in-sample for GP hyperparameter inference. Consequently, this criteria is sometimes called the *predictive log likelihood* (Gelman et al., 2014). The "pointwise" analog (score$_\text{p}$) offers an approximation for the situation where full covariances cannot be derived, as sometimes happens with big testing sets $\mathcal{X}$. For now, we have full $\Sigma(\mathcal{X})$ for all three predictors so Table 1 provides score$_\text{f}$-values. Notice that by score, the GP-MLE hyperparameterization is better, confirming our intuition that the PIs for K-EB are too narrow. Appendix A shows a similar out-of-sample validation exercise comparing kriging to GPs on real data using the Meuse river data (Pebesma, 2009) which is a common 2D kriging data set.

3 Large-scale modeling via localization

Likelihood-based GP inference for hyperparameters (6–8) and prediction (2) requires matrix decomposition for the inverse and determinant of the covariance structure. Most kernels, e.g., Gaussian and Matérn, produce dense K_N (and thus Σ_N), which require $\mathcal{O}(N^3)$ decomposition, say via Cholesky (which furnishes both inverse and determinant). This is prohibitive for N larger than a few thousand. For example, decomposing a single $40,000 \times 40,000$ matrix on a workstation using 8 cores and specialized linear algebra libraries (Intel MKL) takes about 10 minutes. Numerical optimization of hyperparameters might require hundreds of such decompositions in search of the MLE via BFGS. With cubic scaling for larger N, computation time quickly explodes to hours or days. $\mathcal{O}(N^2)$ storage of the $N \times N$ matrix can also become problematic even on the most powerful workstations. Kriging-based inference for hyperparameters via variography bypasses the need to work with an $N \times N$ covariance matrix by binning the data. However, Eq. (2) still requires a dense $N \times N$ inverse to furnish predictions, which is still cubic in computational order.

In the modern age, datasets can easily push into the multimillions and the methods described in Section 2 quickly become infeasible. For that reason, there are increasingly many approaches that

seek a thrifty approximation to GP/kriging models. Heaton et al. (2019) give a thorough comparison of about a dozen recently introduced spatial methods equipped to handle large data. Here we focus on three representative approaches as a means of spanning myriad alternatives in a mining context: Ordinary kriging (OK; Matheron, 1971) is the standard method in mining/geostats which makes local (approximate) prediction after full-data variogram-based hyperparameter estimation; Local Approximate Gaussian Processes (LAGP; Gramacy and Apley, 2015) can be seen as a likelihood-based contemporary analog of OK developed in the surrogate modeling community, making it a natural comparator to OK; finally, the scaled Vecchia approximation (SVecchia) Katzfuss et al. (2021) uses a global approximation to estimate the full covariance structure based on similar locality principles as LAGP/OK. Details for each of these follow in subsections below.

Lastly as a baseline, we consider subset GPs trained via a randomly selected, computationally feasible, $m \ll N$-sized subset of the data points and use them to form an approximation to the full model. Specifically, we build $(X_m, Y_m) \subset (X_N, Y_N)$, using the likelihood for hyperparameter inference via Eqs.(6–8) using (X_m, Y_m) and prediction similarly following (2). We consider m ranging from 1,000 to 8,000; we show later in Figure 8 that $m > 8,000$ is very slow and not competitive with the other methods in terms of accuracy out-of-sample.

3.1 Transductive Modeling

Perhaps the most common solution to big-data matrix issues when predicting via kriging is to deploy what is known as *ordinary kriging* (OK; Matheron, 1971). OK involves using full-data variography to learn kernel hyperparameters, and then a *local* application of that learned kernel through predictive equations (2) conditioned only on a small subset of the data nearby the predictive location(s) of interest. Let $x \in \mathcal{X}$ denote the coordinates of one such location, and $X_m(x) \subseteq X_N$ denote the m "closest" (e.g., via Euclidean distance) members of X_N to x, and let $Y_m(x)$ be the m-associated output values. These are sometimes called the *m-nearest neighbors* (NN) to x in X_N. Then simply apply Eq. (2) with $(X_m(x), Y_m(x))$ rather than (X_N, Y_N). When N is so large that the requisite $N \times N$ matrix decompositions are intractable, choosing $m \ll N$ like $m = 50$ can represent a thrifty-yet-accurate alternative acknowledging that the discarded points $X_N \setminus X_m(x)$ have vanishingly small impact on the predictive equations especially when kernels involve exponential decay.

If a multitude of $x \in \mathcal{X}$ are of interest, these may be processed in serial or, as is increasingly common with modern computing architectures, in parallel on multiple cores of a workstation and/or nodes of a supercomputer. Vast predictive grids $\mathcal{X}$ can be processed efficiently in this manner. There are several variations on this theme, many involving how the "neighborhood" $X_m(x)$ and its size m are defined. For example, one may work with a radius r instead, implicitly defining m depending on the local nature of design locations X_N nearby x. Suitable r from a modeling perspective may be selected by the estimated range R of the semivariogram. However, this does not guarantee a suitably-sized m for all x. One may end up with too small of a neighborhood to make computationally stable calculations/reliable low-variance predictions, or too large of one to be carried out efficiently from a computational perspective. Consequently, there are many hybrids that are often deployed in this space (Wackernagel, 2003, Chapters 11-13).

The idea of tailoring a statistical calculation to a predictive task, using different data and possibly different calculations depending on the predictive location x of interest, is now known as *transductive*

learning (Vapnik, 2013). The transductive moniker is meant to contrast with the more typical *inductive learning* setup where one trains first and predicts second. Under transductive learning, the training happens bespoke to each $x \in \mathcal{X}$, and usually on-demand/in real time. Examples span the gamut of statistical modeling enterprises, often offering both speed and accuracy gains over the inductive analog. Reviewing these would be a distraction here. Instead, we note that OK is an example of transductive learning ahead of its time, albeit a somewhat limited one. Hyperparameter learning with OK is inductive, whereas posterior predictive conditioning is transductive. It is this latter stage where the nonparametric flexibility really comes from, although one might wonder whether things could improve by enhancing the degree transductively, as it were.

A prime example of transductive GP modeling from the wider statistical learning literature is the *local approximate Gaussian process* (LAGP; Gramacy and Apley, 2015). LAGP is similar to OK, using $X_m(x) \subset X_N$ and $Y_m(x)$ analogously for prediction, but it is different in that it extends the notion of locality to hyperparameter inference via the (local) likelihood. That is, the entire process conditions only on $(X_m(x), Y_m(x))$ for inference (6–8) and prediction (2). All inference is off-loaded to numerical optimization. When the response surface is nonstationary, e.g., benefiting by longer lengthscales for some x and shorter for others, LAGP offers enhanced reactivity compared to single, global setting of hyperparameters. Any variation tailored to the full-GP is easy to port to the local setting because LAGP is just many small GPs. Hybrids are possible too. One such example alluded to earlier involves pre-scaling or rotating/projecting (e.g., Wycoff et al., 2021; Sun et al., 2019) to handle non-axis-aligned anisotropy. However, the biggest difference between LAGP and OK does not lie in potential for extension; it is how the neighborhood is defined.

Given fixed m, usually chosen via computational considerations (a common default is $m = 50$), it has been known for sometime that the m-NNs in X_N to x, whether via Euclidean distance or otherwise, do not comprise of an optimal conditioning set $(X_m(x), Y_m(x))$ under any reasonable criteria (e.g., Stein et al., 2004). Example criteria include (Fisher) information about unknown hyperparameters or, as is usually more relevant when predictive accuracy is concerned, predictive uncertainty (a.k.a., mean-squared prediction error). We note that this, in turn, means that the OK predictor is also sub-optimal as a transductive learner. However searching for the best conditioning set $(X_m(x), Y_m(x))$, again under almost any criteria, represents a computationally daunting task because there are $\binom{N}{m}$ alternatives to explore.

Here, another modern statistical learning idea comes in handy: *active learning* (AL). AL is a branch of reinforcement learning/optimal control, or may be viewed as a modernization of old-fashioned sequential design of experiments. In the AL literature, one can often show that a one-step-at-a-time, *greedy* selection of training data is nearly as good as an exhaustive optimization of some criteria by demonstrating that the criteria has a *submodularity* property (Wei et al., 2015). For example, it can be shown that repeatedly acquiring training data (x_{n+1}, y_{n+1}) such that x_i maximizes the predictive variance $x_{n+1} = \arg\max_x \sigma_n^2(x)$ of a GP (2) or neural network model training only on $\{(x_i, y_i)\}_{i=1}^{n}$ obtained previously (e.g., via similar greedy optimization), well-approximates a so-called maximum entropy design, i.e., maximizing Shannon information about unknown hyperparameters (GP lengthscales) for the entire selection $i = 1, \ldots, N$, say. This idea is due to MacKay (1992) for neural networks, and dubbed ALM by Seo et al. (2000) in extension to GPs.

Intuitively, selecting points which have maximum variance will result in a space-filling design because variance is higher away from the training data. Also, intuitively spreading points out will

increase accuracy and reduce uncertainty throughout the input space. But this is coincidental. Guaranteeing reduced predictive variance everywhere, or at a particular location (for choosing an LAGP neighborhood), requires a criteria that squarely targets reduced variance in the region of interest. A common choice is integrated mean-squared predictive error (IMSPE; Sacks et al., 1989):

$$\text{IMSPE}(x_{n+1}) = \int_{\mathcal{X}} \sigma_{n+1}^2(x) \, dx \approx \sum_{x \in X_{\text{ref}}} \sigma_{n+1}^2(x) = \text{ALC}(x_{n+1}, X_{\text{ref}}). \qquad (13)$$

The integral is usually taken over the entire input space, but $\mathcal{X}$ could be any set. This could be interpreted as a criteria for the entire design $X_{n+1} = [X_n; x_{n+1}]^\top$, or simply to select the next input x_{n+1} in an active learning context: $x_{n+1} = \text{argmin}_{x \in \mathcal{X}} \text{IMSPE}(x)$. Due to submodulatirty, both (approximately) optimize the IMSPE criteria over all X_{n+1}. Cohn (1996) developed this for neural networks, and Seo et al. (2000) extended it to GPs. Notice that ALC approximates the integral as a quadrature over a discrete reference set X_{ref}. This is not necessary for GPs, because the integral is analytic when following Eq. (2), but it is for neural networks.

For LAGP, the goal is to get as accurate of a prediction at x as possible, which can be interpreted as a singleton $\{x\} = \mathcal{X} = X_{\text{ref}}$, effectively discarding the sum or integral. We can select a new $x_{n+1} = \text{argmin}_{x_{n+1}} \text{ALC}(x_{n+1}, x)$, and repeated applications will approximate a "local" optimal design for predicting at x. This would usually be applied for selecting new training data in an AL context, but for LAGP we already have a fixed training data set (X_N, Y_N) and so we desire a subsample instead: $x_{n+1} = \text{argmin}_{x_{n+1} \in X_N \setminus X_n} \text{ALC}(x_{n+1}, x)$, which is even easier than a continuous search potentially everywhere in the input space.
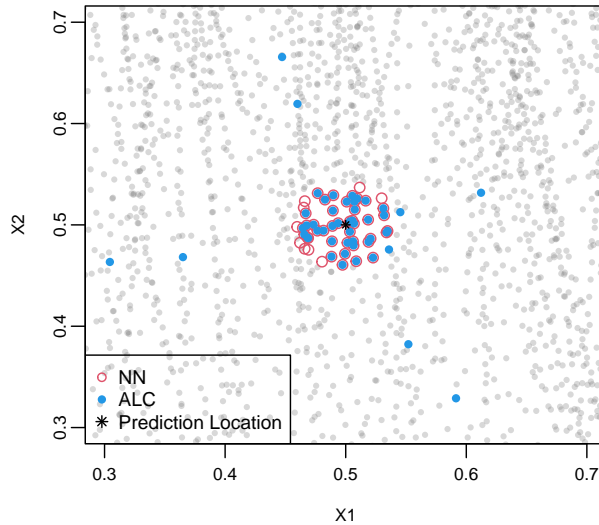

Figure 5: ALC neighborhood for $n = 50$ on simulated borehole data.

In practice, early ALC acquisitions (small n) result in neighborhoods that are indistinguishable from NN. However, later acquisitions (larger n), after many NNs have been conditioned upon near x, the local ALC/IMSPE criteria prefers acquiring "satellite" points farther away. Intuitively, information farther afield becomes more valuable as NNs accumulate near x: you want x_{n+1} to be both close to x but far from X_n. At the start the former dominates, but eventually the latter has

higher weight in the criteria. The end result for $n = 50$, seen in Figure 5, involves ten or so satellite points, departing from an OK or NN subdesign set of the same size.

To a certain extent, LAGP has a "chicken or the egg" problem when dealing with anisotropy. Neighborhoods selected for x are based on Euclidean distance to determine hyperparamters, like $\hat{\theta}_k(x)$, but those values control notions of distance differently in each input coordinate through the kernel. OK experiences this problem too, albeit to a lesser extent when anisotropy is handled by the practitioner as a pre-processing step. Several remedies have been proposed. The original LAGP paper (Gramacy and Apley, 2015) suggested initializing with a default, isotropic θ_0 for all testing locations x, upon which neighborhoods are built (e.g., via ALC) and local, anisotropic local $\hat{\theta}(x)$ are learned through local MLEs separately for each x. This can then be repeated, with neighborhoods based on those $\hat{\theta}(x)$, until things stabilize. Subsequently, a simpler/better approach was promoted by Sun et al. (2019) that is more akin to OK pre-processing, but still completely automated. Liu and Hung (2015) showed that unbiased (global) lengthscales $\hat{\theta} = (\hat{\theta}_1, \ldots, \hat{\theta}_d)$ can be estimated via MLEs from carefully constructed data subsets of large X_N without expense cubic in N. Once these have been learned, they can be used to pre-scale inputs X as $X_k/\sqrt{\theta_k}$ so that the implied MLE global lengthscale is $\hat{\theta}_0 = 1$ under squared-distance kernels like in Eq. (4). In this transformed space, Euclidean distance can be used to determine neighborhoods. This pre-scaled LAGP has become the default setup, and has since been extended to other input "warpings" by Wycoff et al. (2021).

Taken as a predictive field over a densely gridded testing set of x-values, both OK and LAGP (NN or ALC) are discontinuous. Prediction at each point $x \in \mathcal{X}$ is processed independently, both in a statistical and computation sense. So two testing locations right next to each other may have substantively different predictions (in mean and/or variance) because different neighborhoods are used for conditioning. This can be an asset when the response surface exhibits regime/abrupt changes. In tamer, more stationary settings, a non-smooth prediction could be detrimental to statistically efficient and aesthetically pleasing analysis.

3.2 The Scaled Vecchia Approximation

The Vecchia GP approximation (Vecchia, 1988) borrows the neighborhood idea while providing a global model for smooth predictions. It relies on a familiar identity for joint distributions:

$$p(y) = p(y_1)p(y_2|y_1)\ldots p(y_n|y_1, y_2, y_3, \ldots y_{n-1}) = \prod_{i=1}^{N} p(y_i|y_{k(i)}) \quad \text{where} \quad k(i) = \{j : j < i\} \quad (14)$$

$$\approx \prod_{i=1}^{N} p(y_i|y_{c(i)}) \quad \text{where} \quad c(i) \subset k(i)$$

The first line above (equality) is true for any re-indexing of the variables $y = y_1, \ldots, y_n$, and for any y – not specifically for GPs. The approximation (second line) arises from dropping some of those conditioning variables. Let m denote the maximum size of those sets, i.e., so that $|c(i)| = \min(i - 1, m)$, controlling the fidelity of the approximation – more severely for $m \ll i$. The quality of this approximation is determined by the indexing (i.e., the ordering of the conditionals), size m, and which of the conditioning variables $k(i)$ are dropped in $c(i)$ when $m < i$.

Specifically for GPs, one may view the likelihood (6), in this context:

$$L(\phi; Y_N) \approx \prod_{i=1}^{N} L(\phi; y_i | y_{c(i)}) \tag{15}$$

$$= (2\pi)^{-\frac{N}{2}} \left(\prod_{i=1}^{N} \sigma_i^2 \right)^{-\frac{1}{2}} \exp \left\{ - \sum_{i=1}^{N} \frac{1}{2\sigma_i^2} (y_i - \Sigma(x_i, X_{c(i)}) \Sigma(X_{c(i)}, X_{c(i)})^{-1} y_{c(i)})^2 \right\}$$

where $\Sigma(\cdot, \cdot)$ is defined as in Section 2.1 and $\sigma_i^2 = \Sigma(x_i, x_i) - \Sigma(x_i, X_{c(i)}) \Sigma(X_{c(i)}, X_{c(i)})^{-1} \Sigma(X_{c(i)}, x_i)$ is the predictive variance at location i given the conditioning set, $c(i)$. Since distance in the input space, via $\Sigma(\cdot, \cdot)$ is fundamental to GP inference and prediction, one can think of $c(i)$ as defining a "neighborhood." In that context it makes sense (as it did for OK and LAGP) to include in the neighborhood those indices whose input values $X_{c(i)}$ are closer to x_i.

Eq. (15) is similar to (6) except instead of performing one $N \times N$ matrix decomposition (for inverse and determinant) in $\mathcal{O}(N^3)$ time, the Vecchia approximation involves N smaller inversions of $m \times m$ matrices, requiring $\mathcal{O}(Nm^3)$ flops. If m is small, typically between 10 and 25 (Datta et al., 2016; Katzfuss et al., 2021), $\mathcal{O}(Nm^3)$ is quasilinear in N (Katzfuss et al., 2020a). Further computational gains can be realized through sparse-matrix libraries and parallelization by re-writing the likelihood through a Cholesky decomposition of the precision matrix of Y_N, denoted as U:

$$L(\phi; Y_N) \approx (2\pi)^{-\frac{N}{2}} \left(\prod_{i=1}^{N} \sigma_i^2 \right)^{-\frac{1}{2}} \exp \left\{ -\frac{1}{2} \sum_{i=1}^{N} (Y_N^\top U_i U_i^\top Y_N) \right\} \tag{16}$$

$$= (2\pi)^{-\frac{N}{2}} |UU^\top|^{\frac{1}{2}} \exp \left\{ -\frac{1}{2} (Y_N^\top UU^\top Y_N) \right\},$$

where U_i is a $1 \times N$ vector whose j^{th} entry is:

$$U_i^{(j)} = \begin{cases} \frac{1}{\sigma_i} & i = j \\ -\frac{1}{\sigma_i} \left(\Sigma(x_i, x_j) \left(\Sigma(X_{c(i)}, X_{c(i)})^{-1} \right)^{(j,j)} \right) & j \in c(i) \\ 0 & \text{otherwise.} \end{cases} \tag{17}$$

Observe that there are no $N \times N$ matrix decompositions involved, and that any inverses are implicit in the Cholesky factor $UU^\top$, which is sparse.

One may maximize the likelihood (16) to estimate hyperparameters Guinness (2018). Prediction follows the classical setup (2), forming $Y(\mathcal{X}) \mid Y_N$ by stacking training and testing responses:

$$\begin{bmatrix} Y_N \\ Y(\mathcal{X}) \end{bmatrix} \sim \mathcal{N}_{N+N'} \left(\begin{bmatrix} 0 \\ 0 \end{bmatrix}, \begin{bmatrix} UU^\top = \sum_{i=1}^{N} U_i U_i^\top & \sum_{i=1}^{N} U_i \sum_{i=1}^{N'} U_i'^\top \\ \sum_{i=1}^{N'} U_i' \sum_{i=1}^{N} U_i^\top & U'U'^\top = \sum_{i=1}^{N'} U_i' U_i'^\top \end{bmatrix}^{-1} \right).$$

Here we have introduced a new $N' \times N'$ matrix, U' following Eq. (17), via $\mathcal{X}$ rather than X_N. Then, the analog of Eq. (2) yields

$$\mu_N(\mathcal{X}) = -(U'U'^\top)^{-1} \sum_{i=1}^{N'} U_i' \sum_{i=1}^{N} U_i^\top Y_N \quad \text{and} \quad \Sigma_N(\mathcal{X}) = U'U'^\top. \tag{18}$$

18

So the Vecchia GP approximation provides a full joint distribution. Moreover, a single prediction ($\mathcal{X} \equiv \{x\}$), after training, requires just $\mathcal{O}(m^3)$ additional time (Katzfuss et al., 2021), assuming cached values of U. A total of $\mathcal{O}((N' + N)m^3)$ flops are required for inference and prediction, as opposed to $\mathcal{O}(N'^3 + N^3)$ for an ordinary GP.

All that remains is to determine the ordering of indices i in y_i and the composition of the neighborhood sets $c(i)$, since not all choices (when $m \ll n$) lead to equally good approximations (14–15). One option is to follow the LAGP playbook and attempt to optimize over these variables. However this has proved elusive in the literature because an exhaustive search over alternatives would be combinatorially cumbersome, and there is no obvious greedy approach that enjoys submodularity for active learning. Nevertheless there are rules of thumb that make sense intuitively. Many orderings work well (Stein et al., 2004; Guinness, 2018; Katzfuss and Guinness, 2021), but there is a consensus in the literature (Stroud et al., 2017; Datta et al., 2016; Wu et al., 2022) for random indexing. Likewise, those authors prefer NN conditioning sets $c(i)$ comprised of indices $j < i$ whose x_j-values are closest to x_i. This choice has been dubbed NNGP by Datta et al. (2016), although it is important to note that NN are not being used in the same way as LAGP or OK.

Since distances are involved in NN calculations, the Vecchia approximation faces the same "chicken or the egg" problem as LAGP in the face of anisotropy. To help, Katzfuss et al. (2021) describe a scheme similar to pre-scaling for LAGP which updates lengthscales $\hat{\theta}_k$ via Fisher scoring (Osborne, 1992), then re-scales inputs so that NNs can be recalculated, and repeats. Katzfuss et al. (2021) call this "scaled Vecchia" (SVecchia), and argue that it works best with a maximin (Johnson et al., 1990) indexing. We adopt SVecchia as our preferred variation on this theme, in part because it is neatly packaged in software [Section 4].
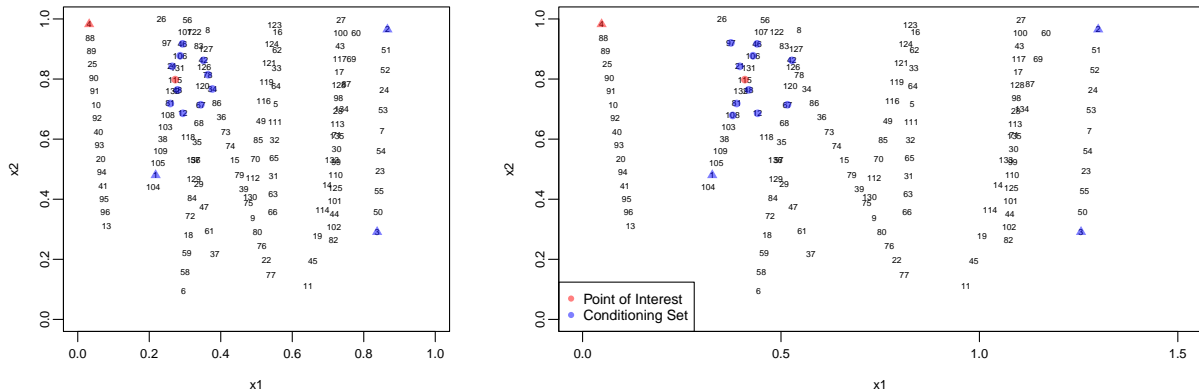

Figure 6: Conditioning sets for two inputs using $m = 10$: point 4 (triangles) and 115 (circles). Left shows the original space in coded inputs, and right shows x_1 pre-scaled by $1/\sqrt{\theta_1} = 2/3$.

Figure 6 shows an illustration using simulated borehole data, providing conditioning sets of size $m = 10$ for two points, labeled with indices $i = 4$ (triangles) and $i = 115$ (circles) respectively. The left plot shows what the conditioning sets look like in the raw, unscaled space while the right is after scaling x_1 by $\frac{2}{3}$; both using the same maximin ordering for easy comparison. The scaling has no effect on the small indices, since point 4, for example, can only condition on $k(4) = c(4) = \{1, 2, 3\}$. See that the lower indices in $c(4)$ (purple triangles) are spread out through space due to maximin ordering. However, point 115 has $|k(115)| = 114$ points to choose from for it's neighborhood $c(115)$.

19

Consequently, the conditioning sets are different between the unscaled and scaled versions. Observe that point 97 is closer than point 34 in the scaled plot, but farther in the unscaled plot.

4   Empirical evaluation on ore data

Here we shall expand on our out-of-sample analysis from Section 2.5 in order to illustrate how modern approximate GP and kriging alternatives [Section 3] compare on two, real and large-scale ore data sets. The layout is as follows. We first introduce the data, evaluation metrics, and detail software in Section 4.1. Section 4.2 presents our validation apparatus, which offers a subtle twist on conventional methods to respect the borehole nature of data acquisition/measurement. Here we also provide results from our first sets of comparisons. Finally, Section 4.3 presents one of several potentially more nuanced analyses that, we believe, is only possible (with ease) in the fully probabilistic GP setting: coping with left-censoring prevalent in ore measurements.

4.1   Implementation details

Our ore data involve three-dimensional inputs, indicated as longitude, latitude and depth in standard units. Although these data record measurements (potential ore outputs) for multiple elements, our analysis here focuses on (log) gold concentration in parts per million. The two data sets are for geographically disparate mining sites that are characterized by different ore forming processes. The first one records more than 150,000 measurements from approximately four-thousand boreholes; the second has $N \approx 500,000$ from 8,000 holes. The second data set also has a substantial number of left-censored values (i.e., thresholded measurements below the detection limits of the apparatus used to sample the core). For example, about 40% of the gold measurements in these data are recorded as 0.05. There are a smaller number of higher limiting values as well. We shall detail how we handle this with two different treatments in Sections 4.2 and 4.3. We are deliberately being vague about many aspects of our data in order to honor confidentiality agreements with mine operators.

We wish to draw an out-of-sample comparison between the methods in Section 3 on these data. In addition to RMSE and proper score (11–12), we also report time, considering both compute (machine) time and practitioner (human) time. Machine time is measured precisely, in seconds, for execution on an eight-core hyperthreaded Intel Core i9-9900K CPU at 3.6GHz with 128GB RAM and Intel MKL linear algebra subroutines. Human time is more subjective/imprecise, and we shall have more to say about that in due course. It is worth remarking that none of the small-data/exact methods from Section 2 are applicable when $N \gg 10,000$, as we have here. Approximation is essential. One simple option is to (randomly) subset the data to a manageable size and apply exact inference on that subset. We consider variously sized "subset GPs" as a benchmark.

For the approximate methods of Section 3, we leverage the following software libraries. The `laGP` package (Gramacy, 2016) for `R` (R Core Team, 2021) on CRAN accommodates subset GP, LAGP, and SLAGP. Its implementation is primarily in `C`, with `OpenMP` for symmetric multi-processing (SMP) parallelization. Only Gaussian kernels are supported by this software. We use defaults throughout, including ALC neighborhoods of size $m = 50$. An SVecchia implementation is provided

by Katzfuss et al. (2021),[3] which piggy-backs off of two R packages: `GpGp` (Guinness, 2018) and `GPVecchia` (Katzfuss et al., 2020b). Although primarily in R under-the-hood, `Rccp` (Eddelbuettel and François, 2011) is used for key subroutines. These, and other calculations based on sparse matrix libraries (Bates et al., 2022) for efficient linear algebra, are also SMP parallelized, although to a lesser degree compared with `laGP`. Here we use the Matèrn kernel and other defaults throughout, including a conditioning set size of $m = 25$. Conventional pre-processing is used to code spatial inputs to the unit 3-cube as recommended by both `laGP` or `SVecchia` documentation.

OK is provided by `GSLIB` (Deutsch and Journel, 1997), which is in Fortran assisted by a shell scripting interface. Whereas the other methods are plug-and-play modulo with few choices that are largely relegated to defaults, interacting with GSLIB is a human-intensive endeavor, involving extensive pre-processing. For example, the analyst must first generate an experimental semivariogram (9) before fitting a positive-definite kernel function. When anisotropic spatial correlation is suspected, the analyst may also have to prepare a variogram map to identify the principal directions of spatial continuity, and then generate experimental semivariograms for two or three directions. This task is also complicated by numerous choices that are part of the analysis, e.g., angular tolerances for directional search windows and different models for spatial autocorrelation (exponential, spherical, Gaussian, etc.) When the variogram analysis is complete, the analyst may also have to complete a coordinate axis rotation to align the dataset with the directions of maximum and minimum spatial correlation, and also experiment with numerous choices for the OK algorithm itself, e.g., search window size and shape, minimum/maximum observations to be use for each estimate. When working with spatially isotropic data, pre-processing may require only an hour or so of additional work; this time expense increases dramatically when faced with anisotropic data.

4.2 Validation exercise

As mentioned in Section 2.5, it is important to compare metrics (11 & 12) on out-of-sample data. Unlike Section 2.5, when dealing with real data, we cannot calculate these metrics on a dense grid spanning the entire input space. In practice, out-of-sample validation occurs by training the model on 90% of the data and testing on the other 10%. Appendix A shows this more in depth. Repeating that randomization multiple times mitigates the so-called Monte Carlo (MC) error metrics like RMSE and score. Here we use $K = 10$-fold *cross validation* (CV; Hastie et al., 2001, Chapter 7) to average over train–test partitions while controlling MC error further by ensuring that each data element is used exactly once for testing, and complementarily exactly nine times for training. CV commences by first shuffling the data, and then evenly dividing it into a partition of K mutually-exclusive *folds*, then iterating over those folds $k = 1, \ldots, 10$, forming a testing set of the data in the kth fold while taking the complement as the training set. In this way, K metric evaluations (like RMSE, score or time) can be calculated and summarized for comparison.

Early attempts at a CV evaluation of the methods in Section 3, after this fashion, revealed a shortcoming in the context of our borehole-driven ore data sets. Namely, the best predictors of a particular held-out testing element were almost always comprised entirely of members of the training data coming from the same borehole. With boreholes "holding" approximately thirty to sixty data elements each, depending on the hole and the data set, this meant that it was highly probable that

---

[3]https://github.com/katzfuss-group/scaledVecchia

an accurate prediction could be made trivially just by those nearby evaluations. This conveyed a substantial advantage to OK and LAGP. We determined that it would be more realistic, and more fair, to hold out entire boreholes for testing, rather than partitioning the data on individual data elements regardless of which borehole they were in. The idea is to simulate what might happen if we were to predict measurements for a new borehole that has not been drilled yet.

Toward that end, we built a custom CV which randomly partitioned our data into K folds of roughly equally-sized boreholes instead. In this way, boreholes are "tested" all at once, without being able to lean on other data within the same borehole for training. Figure 7 shows one such
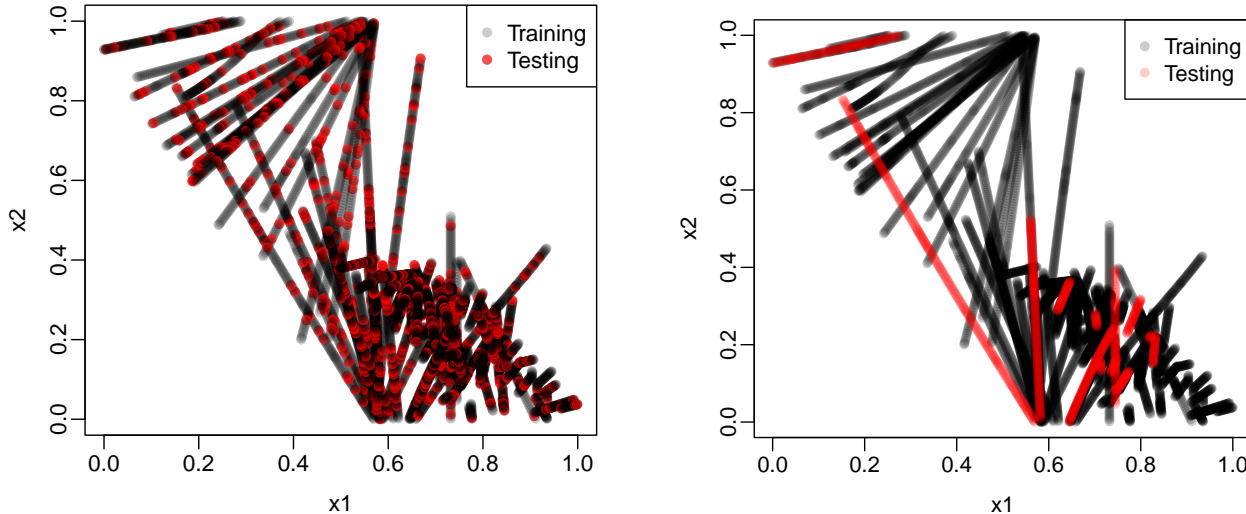

Figure 7: Testing and training sets for the 2d project from Figure 1 with ordinary CV on the left and borehole-preserving CV on the right.

training and testing partition via a single fold of this "borehole-preserving CV." Finally, it is worth remarking that all of our comparator methods use exactly the same CV folds.

Ore data set one

With this setup, Figure 8 shows log RMSE (11), score (score$_p$ from Eq. (12)) and compute time for each of our methods for the first, smaller data set. The big takeaways are that SVecchia, OK and SLAGP are all competitive with each other in terms of RMSE; SLAGP and SVecchia are competitive in score with similar medians. Observe that SLAGP improves upon ordinary LAGP for both RMSE and score. Score for OK could not be calculated because GSLIB does not furnish predictive variances. GSLIB provides standard errors on the mean of the prediction, but those can substantially under-estimate out-of-sample variance. In terms of time, SVecchia takes seconds and LAGP takes a couple minutes to run, both with essentially zero "human time." We report that OK takes several hours of human time to perform a variography analysis, choosing between competing kernel formulations and parameterization and to determine an appropriate rotation and pre-scaling of the data in order to cope with an otherwise isotropic formulation. After that has been done, training and prediction takes about the same amount of time as (S)LAGP. It is interesting
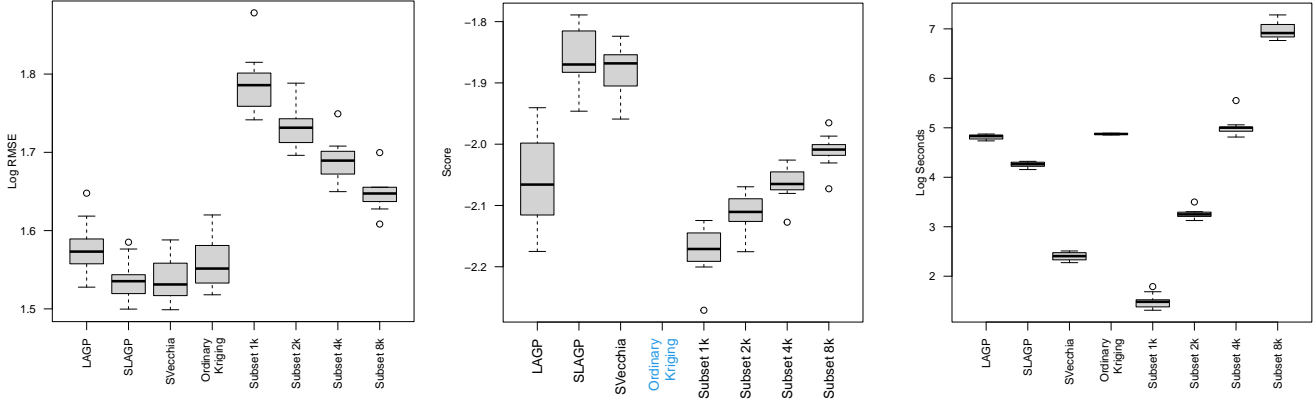
22

Figure 8: Drillhole-presererving 10-fold CV summary for the first data set. Left: RMSE (smaller is better); Middle: score$_p$ (higher is better). Right: compute time (smaller is better).

that SLAGP is faster than LAGP despite involving more algorithmic steps: first fit a global subset model, then local models on transformed inputs. The explanation is that, after pre-scaling, local MLE calculations are easier: they require many fewer iterations to converge. Computation time for the subset-GP methods explodes with $\mathcal{O}(m^3)$ flops as m grows.

Our conclusion from this experiment is that, although SLAGP edges out SVecchia on accuracy and UQ for this problem, SVecchia is slightly better overall because of its substantially lighter time commitment. However, for an individual (or entire borehole) prediction, SLAGP times are orders of magnitude faster – the times in the right panel of Figure 8 are for all boreholes in the fold – because each calculation is independent of others. For a one-off prediction it is the clear winner. Although raw accuracy is similar compared to OK, the modern GP methods are hands-off, provide full UQ, and are faster to train/predict.

Ore data set two

A similar analysis for the second, larger data set, is nuanced because of the substantial left-censoring. One option is to ignore the censoring and treat the recorded values as the actual values. If there were a small number of such values, sporadically located in the input space, this might work well. However, there are a sizable number (more than 40%), and they cluster nearby one another. Having some responses smoothly vary in the input space, with others "flatlining" at 0.05, say, for most or all of a borehole represents an almost pathological contrast to typical smoothness assumptions underlying GP (and kriging) methods. So to start with, we removed these values, and dealt with borehole-preserving CV only on the remaining 259,555 data records. In Section 4.3 we shall discuss an imputation scheme for bringing these observations back into the folds. The remaining data still contain a moderate degree of left-censoring which we largely ignore except when an entire borehole contains the same (thresholded) gold response. In that case, we collapse those records into three data points – two ends and midway point – all with the same gold value. This collapsing is especially important for LAGP and OK because, due to their local nature, those methods occasionally have neighborhoods consisting of data from one or two boreholes only. If those measurements lack diversity due to thresholding, training can result in numerical singularities.
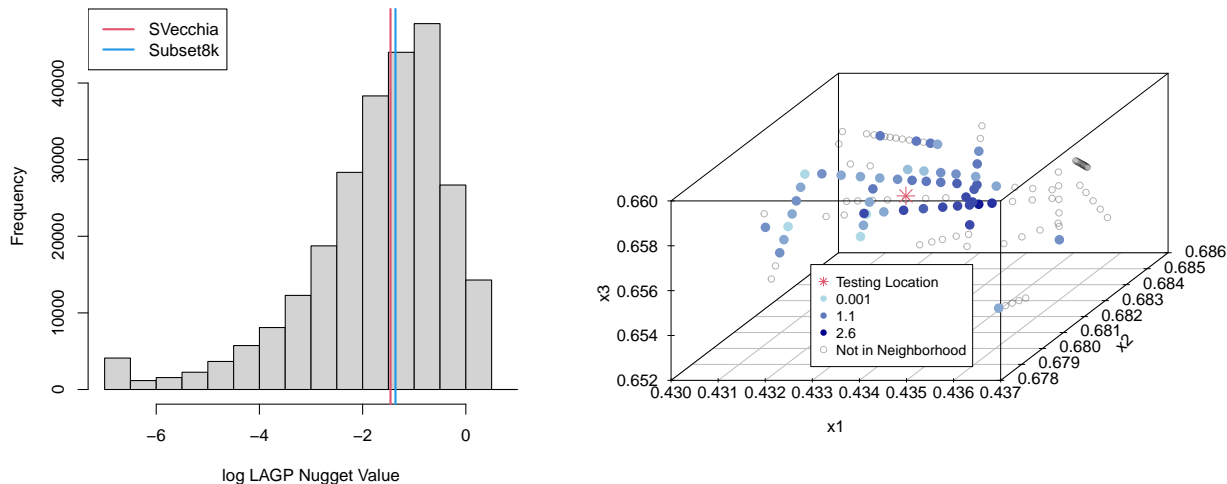
23

Figure 9: Left: Histogram of log LAGP nuggets with SVecchia and subset8k nuggets. Right: An example neighborhood using LAGP's ALC for a point with low estimated variance.

Even after such modifications, we found that LAGP and OK struggled to predict at some testing sites. `GSLIB`, implementing OK, would simply refuse to provide a prediction in these instances, or similarly when there are no training data points within a user-specified radius (regardless of m), returning an error code. In these data, that amounts to about 300 testing sites per fold. The `laGP` software would furnish a prediction, but when comparing the corpus of other predictions in a fold it was obvious that something was amiss, particularly with the estimated (local) nugget parameter and, consequently, the predicted variance. To investigate, we plotted a histogram of the estimated nuggets from all of the local fits, shown in the left panel of Figure 9, and compared these against the global nugget(s) provided by subset and SVecchia methods. We observed that occasionally, local nuggets were being estimated at the lower-threshold imposed by the `laGP` default search range (leftmost-bin in the histogram). The local neighborhood for one, representative member of this group is shown on the right panel of the figure. Observe that most of the points nearby have log gold values above 1 (are similar shades of blue) with some satellite points having lower log gold values. Thus a prediction of log gold a bit higher than 1 with low variance makes sense. However, the true log gold value for this point is about 0.1, meaning the prediction is confident and wrong – which would lead to a poor score evaluation.

Of course, we cannot know this location provides a bad prediction until we look at the testing value for this predictive location. So we decided to replace local nuggets estimated at the lower-bound of `laGP`'s' search range with the median of the nuggets from the rest of the distribution. This led to a substantial improvement in out-of-sample scores, described momentarily. If this sounds *ad hoc*, that is because it is. But a prediction with UQ that is based on compromise and a limited degree of post-hoc human intervention is better than no prediction at all (OK/`GSLIB`).

Figure 10 shows these results with black boxplots. (The red ones involve a study on imputation in Section 4.3, so ignore those for now.) The story is similar to the first data set in Figure 8: SLAGP, SVecchia, and OK outperform subsetting in terms of RMSE. Here, OK appears to be the most accurate, but these RMSE calculations do not include any error-coded outputs (representing more than 300 presumably "bad" predictions per fold). So this is not a holistic assessment of OK
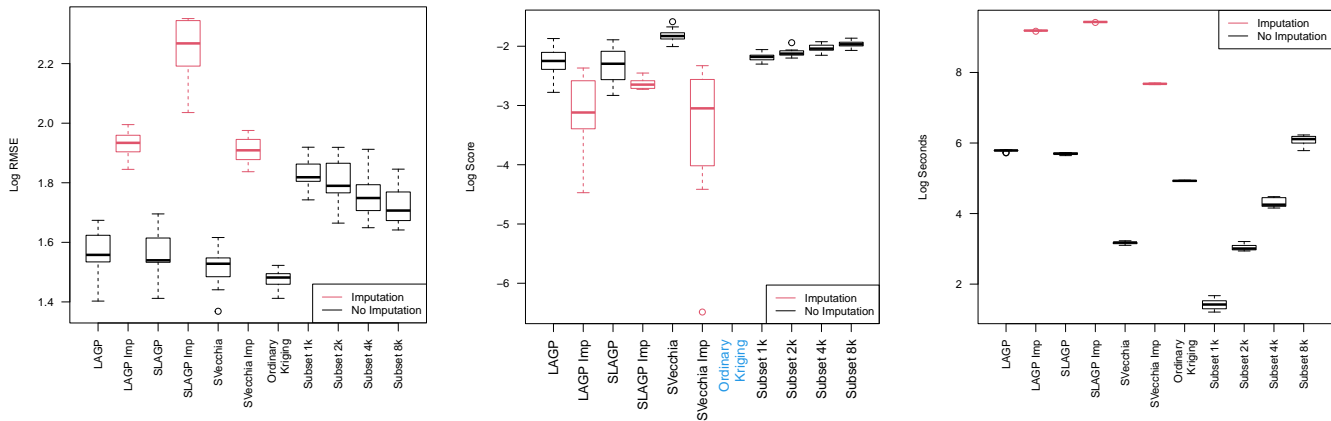
Figure 10: Drillhole-preserving 10-fold cross validation summary for the first data set. See Figure 8 caption. Red boxplots are discussion in Section 4.3.

accuracy. By score, which again cannot be calculated for OK, SVecchia is the clear winner, and the second-fastest in this comparison. (S)LAGP, which is similar in spirit to OK, has inferior scores despite modifications to address stability issues to do with the nugget (above).

4.3 Imputation

It is unsatisfying to discard data. Even a coarsely left-censored value contains information, which can be used to enhance training. Perhaps even more importantly, one may wonder how accurately those censored values may be predicted, thereby increasing the resolution of those measurements, by borrowing information from higher-accuracy (training) data measurements nearby. This is a standard enterprise in statistical learning when fully probabilistic generative modeling, like the GP, is used. There are many options when handling "missing data," of which censoring is one example (Schafer, 1997; Little and Rubin, 2002).

One way to incorporate censored ore values, without destroying smoothness or stationarity assumptions underlying GP spatial models, is through *imputation* (e.g., Little and Rubin, 2002, Chapter 5). In our context, imputation basically means generating a plausible response Y-value for censored locations that both respects the censored measurement, and the smoothness of the underlying spatial field learned through other, completely observed data. Once generated, the imputed value may be treated as if it were a completely observed value going forward, say for prediction. Of course, treating an imputed value as observed ignores the uncertainty in the imputation. *Multiple imputation* acknowledges that uncertainty by randomly imputing several possible values and performing inference based on the corpus of those imputed values, e.g., through averaging.

Illustrating how this could work in our ore context requires some notational scaffolding. Let $D_N = (D_{\mathrm{obs}}, D_{\mathrm{cens}})$ represent the partition of the complete data set into its fully observed and censored components, respectively. For example, $D_{\mathrm{obs}} = (X_{\mathrm{obs}}, Y_{\mathrm{obs}})$, may be the portion of the second data set we were working with in Section 4.2, and $D_{\mathrm{cens}} = (X_{\mathrm{cens}}, Y_{\mathrm{cens}})$ was the part we (temporarily) discarded. Imputed values $Y_{\mathrm{imp}}(X_{\mathrm{cens}})$, may be used to augment D_{obs} to obtain

$D_{\text{imp}} = (D_{\text{obs}}, (X_{\text{cens}}, Y_{\text{imp}}))$ via truncated Gaussian simulation

$$Y_{\text{imp}} \sim \mathcal{N}_{N_{\text{cens}}}(\mu_{\text{obs}}(X_{\text{cens}}), \Sigma_{\text{obs}}(X_{\text{cens}}))\mathbb{I}_{\{Y_{\text{imp}} \leq Y_{\text{cens}}\}}, \tag{19}$$

where $\mathbb{I}_{\{Y_{\text{imp}} \leq Y_{\text{cens}}\}}$ is an indicator function, returning 1 if $Y_{\text{imp}} \leq Y_{\text{cens}}$ and 0 otherwise. Quantities $\mu_{\text{obs}}(X_{\text{cens}})$ and $\Sigma_{\text{obs}}(X_{\text{cens}})$ are the predictive moments (2) of a GP fit conditioned on D_{obs}.

Although software exists to sample from a truncated MVN directly (e.g., Wilhelm and G, 2022), such as those in (19), in practice it can be difficult to generate a sufficient number of values below Y_{cens} when N_{cens} is of modest size, for example in the hundreds (Li and Ghosh, 2015). A more customized approach that acknowledges the form of our (approximate/large-scale) spatial surrogates helps. In the (S)LAGP context, we may use Eq. (14) to sample Y_{imp} from the truncated MVN (19) one at a time, conditioning on the previously sampled imputed values and the observed data. LAGP is designed to look at each location in the testing set independently which makes this setup work. On the other hand, SVecchia is designed to give a global model approximation, so doing a similar one-at-a-time conditional imputation is too crude. We instead prefer a bespoke rejection sampling (Casella et al., 2004) scheme that proceeds in epochs: first generate posterior samples from the MVN (19) unconstrained, keeping any values that satisfy the censoring threshold. Then condition on those imputations and the observed values, resampling at locations without an imputed value, repeating until Y_{imp} is completely filled in.

Algorithm 1: Multiple imputation for large scale GPs under left censoring

> **input** D_{obs} and D_{cens} and testing locations $\mathcal{X}$
> **for** $i = 1, \ldots, M$ **do**
>> **if** *(S)LAGP* **then**
>>> $D = D_{\text{obs}}$
>>> **for** $j = 1, \ldots, N_{\text{cens}}$ **do**
>>>> $(\mu, \sigma^2) = \text{(S)LAGP}(D, X_{\text{cens}}[j])$ // LAGP prediction: Sec. 3.1
>>>> $Y_{\text{imp}}[j] \sim N_1(\mu, \sigma^2)\mathbb{I}_{\{Y_{\text{imp}}[j] \leq Y_{\text{cens}}\}}$ // Posterior tnorm draw: Eq. (19)
>>>> $D = (D, (X_{\text{cens}}[j], Y_{\text{imp}}[j]))$ // Imputation step
>>>
>>> $(\mu_i, \sigma_i^2) = \text{(S)LAGP}(D, \mathcal{X})$ // Predict at testing locations
>>
>> **if** *SVecchia* **then**
>>> $D = D_{\text{obs}}$
>>> **while** $|X_{\text{cens}}| > 0$ **do**
>>>> $(\mu, \Sigma) = \text{SVecchia}(D, X_{\text{cens}})$ // SVecchia prediction: Eq. (18)
>>>> $Y_{\text{imp}} \sim N_{|X_{\text{cens}}|}(\mu, \Sigma)$ // Unconstrained posterior MVN draw
>>>> $w = \text{which}(Y_{\text{samp}} < Y_{\text{cens}})$
>>>> $D = (D, (X_{\text{cens}}[w], Y_{\text{imp}}[w]))$ // Imputation step
>>>> $X_{\text{cens}} = X_{\text{cens}} \setminus X_{\text{cens}}[w]$
>>>
>>> $(\mu_i, \Sigma_i) = \text{SVecchia}(D, \mathcal{X})$ // Predict at testing locations
>
> **return** (μ_i, Σ_i), for $i, \ldots, m$ // where $\Sigma_i = \text{diag}(\sigma_i^2)$ for (S)LAGP

Algorithm 1 provides pseudo-code for concreteness, wrapping a single imputation with a `for` to obtain M multiple imputations. Rubin (1987) indicates that M between two and ten works

well, so we use $M = 5$ in our exercises. Each of the M imputed values are plausible realizations of the censored measurements, which correspond to M posterior/predictive Gaussian distributions for each testing location. Thus we may use Gaussian mixture moment equations (Reynolds, 2009) to report the mean and variance predictions for the testing set:

$$\mu_{\mathrm{MI}}(\mathcal{X}) = \frac{1}{M} \sum_{i=1}^{M} \mu_i(\mathcal{X}) \tag{20}$$

$$\sigma_{\mathrm{MI}}^2(\mathcal{X}) = \frac{1}{M} \sum_{i=1}^{M} \sigma_i^2(\mathcal{X}) + \frac{1}{M} \sum_{i=1}^{M} \mu_i^2(\mathcal{X}) - \left(\frac{1}{M} \sum_{i=1}^{M} \mu_i(\mathcal{X}) \right)^2$$

While this cannot completely account for all possible uncertainties due to imputation, because we have not looked at all possible imputation values (only M), we can always increase M if desired. It may be shown that these equations give an unbiased estimate of mean and variance for any M.

Imputation in practice

To begin with an illustration in a simple, controlled setting, the left panel of Figure 11 shows a classical GP model with and without imputation. The true function is $f(x) = 2\sin(4\pi x) + \epsilon$ where $\epsilon \sim \mathcal{N}(0, 0.1)$ and an observation threshold of $y = 1$ with $n = 20$ randomly selected training points. There are two main regions of censoring, one in the center and one at the upper end of inputs. In the center, the model with imputation gets closer in mean to the truth. On the upper end, the variance of our predictions is much lower when conditioning on imputed values. Observe that the model with imputation is a better fit for the true curve.
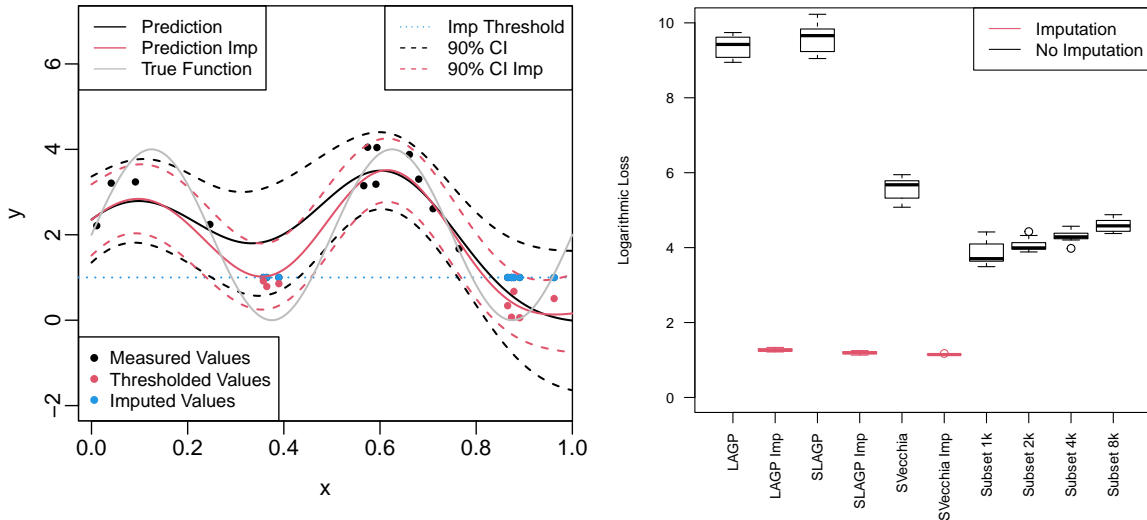

Figure 11: Left: Imputation illustration for 1d synthetic data. Right: CV log loss (21) from ore data set two that are below the detection threshold using big data methods with and without imputation.

When working with real data, we do not have the luxury of knowing what the "true curve" is. Consequently, it is much tougher to assess improvement in the quality of fit through imputation.

RMSE and score on an out-of-sample testing set, say via CV, are problematic because censored data values – as elements of the testing set – are not realizations from the same population as the model/predictive quantities are ($\mu_n(x)$ and $\sigma_n^2(x)$). The only "truth" we know about these points is that they are measured to be below the threshold. The best we can to is determine if the model accurately predicted the "parity" of its recorded value, either above or below the threshold. The GP framework makes this transition simple. The probability of accurate prediction under a threshold may be obtained through inverse Gaussian CDF evaluated at the threshold. The proper scoring mechanism (Gneiting and Raftery, 2007) for such probabilities is the logarithmic loss (LL; Good, 1952), also known as cross-entropy loss in the neural network literature. Lower LL is better. When all of the testing data are from one class (less than Y_{cens}), LL boils down to:

$$\text{LL}(\mathcal{X}_{\text{cens}}) = -\frac{1}{N'_{\text{cens}}} \sum_{x \in \mathcal{X}_{\text{cens}}} \log(\mathbb{P}(Y(x) \leq Y_{\text{cens}}) = -\frac{1}{N'_{\text{cens}}} \sum_{x \in \mathcal{X}_{\text{cens}}} \log\left(\Phi^{-1}(Y_{\text{cens}}; \mu(x), \sigma^2(x))\right). \quad (21)$$

Returning now to our second ore analysis from Section 4.2, we describe our experience with multiple imputation on these data. We only explore (S)LAGP and SVecchia in this context. When dealing with the subset methods, imputation is of limited additional value as completely observed data are plentiful relative to the subset size. It is cumbersome, but not impossible to entertain imputation under OK. Being faithful to the imputation scheme would require human intervention to re-fit variograms after each new imputation is obtained. That would result in over 100K variogram fits in this example! In this context, we see LAGP as an equivalent, automatic variation on OK that can be more easily entertained in an imputation/censored values context.

The right plot of Figure 11 demonstrates that our imputation scheme yields improved LL (21) across the board. For reference, $-\log(0.001) = 6.9$ and $-\log(0.2) = 1.6$, so fits leveraging imputation provide a probability of 0.2 for being below thresholds, on average, compared to 0.001 or worse for the models without imputation. At first, it is hard to square this improvement with what appears to be contrary messaging from the imputation results in Figure 10 (red boxplots). If a practitioner is certain that a particular region is high in gold concentration, *a priori*, then dropping the censored values (i.e., no imputation), which are all low-measurements, leads to more accurate results. Yet dropping thresholded values exposes the practitioner to confirmation bias: predictions appear more accurate in one part of the space at the expense of massive over-predictions in another. This is what the right panel of Figure 11 shows.

5 Conclusion

We have highlighted similarities and differences in GP modeling and kriging. On the one hand, disparate terminology obscures a practically identical modeling apparatus. On the other, approaches to hyperparameter estimation and the treatment of anisotropy can imply drastically different degrees of automation/requisite human intervention. We demonstrated that with smaller training data sets, expert intervention through variography can lead to (slightly) better fits. However, we advocate for taking the human out of the loop even in this situation, and relying on the likelihood. We are not saying the human should be eliminated entirely. Identifiability issues (Tang et al., 2021; Kaufman and Shaby, 2013) inherent in separating signal from noise (i.e., inferring the nugget), and

in determining smoothness (p and ν), mean it is always sensible to inspect outputs and challenge downstream inferences against stylized facts about the system. But intimate human involvement challenges reproducibility and limits scope for extension, such as with with censored data in our mining context. Careful engineering atop of sound principles can improve upon many human labor-intensive tasks – possibly a defining feature of the machine learning approach to statistics.

By introducing modern kriging/GP approximations, we have shown that when working with large mining datasets in low dimension, the scaled Vecchia approximation is faster and at least as accurate as LAGP/OK with the benefit of giving full joint posterior distributions. Throughout, we leveraged off-the-shelf libraries with defaults settings. These represent the tip of an iceberg. See, e.g., Heaton et al. (2019) for a survey of additional modern approaches to modeling spatial data. Mining data often have some non-stationarity due to geological structures, e.g., faults, folds, and fracture networks. Recently it has been suggested that a deep GP (Damianou and Lawrence, 2013; Sauer et al., 2022) may handle such non-stationary data more gracefully than ordinary GPs: combining the accuracy of deep learning (deep neural networks) with the uncertainty quantification (UQ) features of fully probabilistic (GP) modeling.

Finally, GP-based machinery – as opposed to kriging – is less intimately tied to low-dimensional (2-3d) input spaces, allowing for the incorporation of more predictor variables. In the case of mining for gold, measurements for other minerals (in a similar domain) can be used to help build models that are more accurate and give better UQ. This can easily increase the input dimension to the tens of variables. That challenges variography, but the GP approach remains essentially unchanged.

Code Availability. All examples/illustrations can be found on our Git repo on Bitbucket:

https://bitbucket.org/gramacylab/mining_code/src/master/

Data Availability. Data for the illustrative examples in Section 2 is provided either in-line with our code (see git repo above), or as included with an open source library utilized by our code. The mining data from our industrial partners is proprietary and we do not have permission to share it. However, the data is in a standard CSV-column format, and our code for those examples (in the repo above) may be utilized with any data that can be supplied in that form.

Acknowledgements

Declarations

Conflict of Interest. The authors have no competing interests to declare.

References

Abrahamsen, P. (1997). "A review of Gaussian random fields and correlation functions." Norsk Regnesentral/Norwegian Computing Center Oslo, `https://www.nr.no/directdownload/917_Rapport.pdf`.

Banerjee, S. (2017). *Geostatistical Modeling for Environmental Processes*, 81–96.

Bates, D., Maechler, M., and Jagan, M. (2022). *Matrix: Sparse and Dense Matrix Classes and Methods*. R package version 1.4-1.

Byrd, R., Lu, P., Nocedal, J., and Zhu, C. (1995). "A Limited Memory Algorithm for Bound Constrained Optimization." *SIAM Journal on Scientific Computing*, 16.

Casella, G. and Berger, R. (2001). *Statistical Inference*. Duxbury.

Casella, G., Robert, C. P., and Wells, M. T. (2004). "Generalized Accept-Reject Sampling Schemes." *Lecture Notes-Monograph Series*, 45, 342–347.

Cohn, D. A. (1996). "Neural Network Exploration Using Optimal Experiment Design." *Neural Networks*, 9, 6, 1071–1083.

Cressie, N. (1985). "Fitting variogram models by weighted least squares." *Journal of the International Association for Mathematical Geology*, 17.

— (1993). *Statistics for Spatial Data*. Wiley Series in Probability and Statistics. Wiley.

Damianou, A. and Lawrence, N. D. (2013). "Deep Gaussian Processes." In *Proceedings of the Sixteenth International Conference on Artificial Intelligence and Statistics*, eds. C. M. Carvalho and P. Ravikumar, vol. 31 of *Proceedings of Machine Learning Research*, 207–215. Scottsdale, Arizona, USA: PMLR.

Datta, A., Banerjee, S., Finley, A. O., and Gelfand, A. E. (2016). "Hierarchical Nearest-Neighbor Gaussian Process Models for Large Geostatistical Datasets." *Journal of the American Statistical Association*, 111, 514, 800–812. PMID: 29720777.

Deutsch, C. V. and Journel, A. G. (1997). *GSLIB: Geostatistical Software Library and User's Guide*. New York, NY: Oxford University Press.

Diggle, P. J. and Ribeiro, P. J. (2007). *Model-based Geostatistics*. Springer.

Eddelbuettel, D. and François, R. (2011). "Rcpp: Seamless R and C++ Integration." *Journal of Statistical Software*, 40, 8, 1–18.

Gelman, A., Hwang, J., and Vehtari, A. (2014). "Understanding predictive information criteria for Bayesian models." *Statistics and computing*, 24, 6, 997–1016.

Gneiting, T. and Raftery, A. E. (2007). "Strictly Proper Scoring Rules, Prediction, and Estimation." *Journal of the American Statistical Association*, 102, 477, 359–378.

Good, I. J. (1952). "Rational Decisions." *Journal of the Royal Statistical Society. Series B (Methodological)*, 14, 1, 107–114.

Gramacy, R. and Lian, H. (2012). "Gaussian process single-index models as emulators for computer experiments." *Technometrics*, 54, 1, 30–41.

Gramacy, R. and Polson, N. (2011). "Particle learning of Gaussian process models for sequential design and optimization." *Journal of Computational and Graphical Statistics*, 20, 1, 102–118.

Gramacy, R. B. (2016). "laGP : Large-Scale Spatial Modeling via Local Approximate Gaussian Processes in R." *Journal of Statistical Software*, 72.

— (2020). *Surrogates: Gaussian Process Modeling, Design and Optimization for the Applied Sciences*. Boca Raton, Florida: Chapman Hall/CRC.

Gramacy, R. B. and Apley, D. W. (2015). "Local Gaussian Process Approximation for Large Computer Experiments." *Journal of Computational and Graphical Statistics*, 24, 2, 561–578.

Guinness, J. (2018). "Permutation and grouping methods for sharpening Gaussian process approximations." *Technometrics*, 60, 4, 415–429.

Hastie, T., Tibshirani, R., and Friedman, J. (2001). *The Elements of Statistical Learning*. Springer Series in Statistics. New York, NY, USA: Springer New York Inc.

Hastings, W. K. (1970). "Monte Carlo Sampling Methods Using Markov Chains and Their Applications." *Biometrika*, 57, 1, 97–109.

Heaton, M. J., Datta, A., Finley, A. O., Furrer, R., Guinness, J., Guhaniyogi, R., Gerber, F., Gramacy, R. B., Hammerling, D. M., Katzfuss, M., Lindgren, F., Nychka, D. W., Sun, F., and Zammit-Mangion, A. (2019). "A Case Study Competition Among Methods for Analyzing Large Spatial Data." *Journal of Agricultural, Biological, and Environmental Statistics*, 24, 398 – 425.

Johnson, M., Moore, L., and Ylvisaker, D. (1990). "Minimax and maximin distance designs." *Journal of Statistical Planning and Inference*, 26, 2, 131–148.

Jones, D., Schonlau, M., and Welch, W. (1998). "Efficient global optimization of expensive black-box functions." *Journal of Global Optimization*, 13, 4, 455–492.

Kalpić, D. and Hlupić, N. (2011). *Multivariate Normal Distributions*, 907–910. Berlin, Heidelberg: Springer Berlin Heidelberg.

Katzfuss, M. and Guinness, J. (2021). "A general framework for Vecchia approximations of Gaussian processes." *Statistical Science*, 36, 1, 124–141.

Katzfuss, M., Guinness, J., Gong, W., and Zilber, D. (2020a). "Vecchia Approximations of Gaussian-Process Predictions." *Journal of Agricultural, Biological and Environmental Statistics*, 25, 3, 383–414.

Katzfuss, M., Guinness, J., and Lawrence, E. (2021). "Scaled Vecchia approximation for fast computer-model emulation."

Katzfuss, M., Jurek, M., Zilber, D., and Gong, W. (2020b). *GPvecchia: Scalable Gaussian-Process Approximations*. R package version 0.1.3.

Kaufman, C. G. and Shaby, B. A. (2013). "The role of the range parameter for estimation and prediction in geostatistics." *Biometrika*, 100, 2, 473–484.

Li, Y. and Ghosh, S. K. (2015). "Efficient Sampling Methods for Truncated Multivariate Normal and Student-t Distributions Subject to Linear Inequality Constraints." *Journal of Statistical Theory and Practice*, 9, 4, 712–732.

Little, R. J. A. and Rubin, D. B. (2002). *Statistical Analysis with Missing Data, Second Edition*. Wiley-Interscience.

Liu, K., Li, Y., Hu, X., Lucu, M., and Widanage, W. D. (2020). "Gaussian Process Regression With Automatic Relevance Determination Kernel for Calendar Aging Prediction of Lithium-Ion Batteries." *IEEE Transactions on Industrial Informatics*, 16, 6, 3767–3777.

Liu, Y. and Hung, Y. (2015). "Latin Hypercube Design-Based Block Bootstrap for Computer Experiment Modeling." Tech. rep., Rutgers.

MacKay, D. (1992). "Information-based objective functions for active data selection." *Neural Computation*, 4, 4, 590–604.

Matheron, G. (1963). "Principles of geostatistics." *Economic Geology*, 58, 8, 1246–1266.

— (1971). *The Theory of Regionalized Variables and Its Applications*. Fontaineblue, Paris: Les Cahiers du Centre de Morphologie Mathematique.

Osborne, M. R. (1992). "Fisher's Method Of Scoring." *Int. Stat. Rev*, 60, 271–286.

Pebesma, E. (2009). "The meuse data set: a tutorial for the gstat R package."

R Core Team (2021). *R: A Language and Environment for Statistical Computing*. R Foundation for Statistical Computing, Vienna, Austria.

Rasmussen, C. E. and Williams, C. K. I. (2006). *Gaussian Processes for Machine Learning*. Cambridge, MA: MIT Press.

Reynolds, D. (2009). *Gaussian Mixture Models*, 659–663. Boston, MA: Springer US.

Rubin, D. B. (1987). *Multiple Imputation for Nonresponse in Surveys*. New York, NY: Wiley.

Sacks, J., Welch, W. J., Mitchell, T. J., and Wynn, H. P. (1989). "Design and Analysis of Computer Experiments." *Statistical Science*, 4, 4, 409 – 423.

Sauer, A., Cooper, A., and Gramacy, R. B. (2022). "Vecchia-approximated Deep Gaussian Processes for Computer Experiments."

Sauer, A., Gramacy, R. B., and Higdon, D. (2021). "Active learning for deep Gaussian process surrogates." *Technometrics*, , just-accepted, 1–39.

Schafer, J. L. (1997). *Analysis of Incomplete Multivariate Data*. New York, New York: Chapman Hall/CRC.

Seo, S., Wallat, M., Graepel, T., and Obermayer, K. (2000). *Gaussian process regression: active data selection and test point rejection*, 27–34. New York, NY.

Stein, M. L. (1999). *Interpolation of spatial data: some theory for kriging*. Springer Science & Business Media.

Stein, M. L., Chi, Z., and Welty, L. J. (2004). "Approximating likelihoods for large spatial data sets." *Journal of the Royal Statistical Society: Series B (Statistical Methodology)*, 66, 2, 275–296.

Stroud, J. R., Stein, M. L., and Lysen, S. (2017). "Bayesian and maximum likelihood estimation for Gaussian processes on an incomplete lattice." *Journal of computational and Graphical Statistics*, 26, 1, 108–120.

Sun, F., Gramacy, R., Haaland, B., Lawrence, E., and Walker, A. (2019). "Emulating satellite drag from large simulation experiments." *SIAM/ASA Journal on Uncertainty Quantification*, 7, 2, 720–759. Preprint arXiv:1712.00182.

Tang, W., Zhang, L., and Banerjee, S. (2021). "On identifiability and consistency of the nugget in Gaussian spatial process models." *Journal of the Royal Statistical Society: Series B (Statistical Methodology)*, 83, 5, 1044–1070.

Vapnik, V. (2013). *The Nature of Statistical Learning Theory*. New York, NY: Springer-Verlag New York.

Vecchia, A. V. (1988). "Estimation and Model Identification for Continuous Spatial Processes." *Journal of the Royal Statistical Society. Series B (Methodological)*, 50, 2, 297–312.

Wackernagel, H. (2003). *Multivariate Geostatistics: An introduction with applications*. Berlin: Springer.

Wei, K., Iyer, R., and Bilmes, J. (2015). "Submodularity in data subset selection and active learning." In *International Conference on Machine Learning*, 1954–1963. PMLR.

Wendland, H. (2004). *Scattered Data Approximation*. Cambridge, England: Cambridge University Press.

Wilhelm, S. and G, M. B. (2022). *tmvtnorm: Truncated Multivariate Normal and Student t Distribution*. R package version 1.5.

Wu, L., Pleiss, G., and Cunningham, J. (2022). "Variational Nearest Neighbor Gaussian Processes." *arXiv preprint arXiv:2202.01694*.

Wycoff, N., Binois, M., and Gramacy, R. B. (2021). "Sensitivity Prewarping for Local Surrogate Modeling." *arXiv preprint arXiv:2101.06296*.

Appendix A A common 2d kriging example

Consider the Meuse river data, which often serves as a tutorial-level example of kriging (Pebesma, 2009). These data consist of measurements of concentrations of metals in the topsoil of the Meuse river in the Netherlands. Our analysis here focuses on 155 zinc measurements in parts per million (ppm) taken at 2d spatial locations recorded as Rijksdriehoeks Coordinates (National Triangulation Coordinates of the Neatherlands) distributed at varying uniformity along the river. To prepare the data for analysis, we follow the statistical learning/surrogate modeling practice of coding these inputs as X_N in the unit cube $[0,1]^2$ and model the centered (i.e., empirically mean adjusted) natural logarithm of zinc concentration as the response. This automatic pre-processing step helps initialize the numerical solvers for hyperparameters at default settings, and makes a Gaussian assumption on the response more compatible.

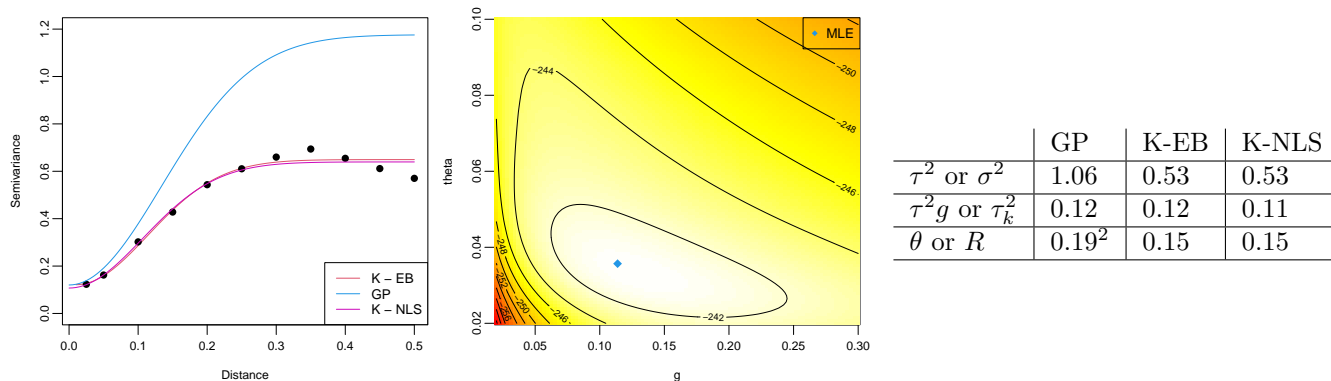|	GP	K-EB	K-NLS
τ^2 or σ^2	1.06	0.53	0.53
$\tau^2 g$ or τ_k^2	0.12	0.12	0.11
θ or R	0.19^2	0.15	0.15

Figure 12: Left: Variogram for kriging by eye in red, kriging by NLS in purple and GP in blue. Middle: GP log MLE surface with optimum in blue. Right: Table comparing hyperparameters.

Figure 12 shows the variogram and MLE-based analysis in views similar to Figures 3 and 4 for these data. Observe that the empirical semivariogram is much better behaved, compared to our first example, and that consequently EB and NLS hyperparameter estimates and variogram fits are quite similar. The main difference between the GP and these kriging alternatives is that the estimated scale hyperparameter τ^2 is much larger. With similar nuggets and lengthscales, the rate of increase in the variogram is about the same, but reaching a higher level. Since the estimated scale does not impact the predictive mean $\mu(\mathcal{X})$, see Eq. (2), it is perhaps not surprising that the predictive surfaces (via $\mathcal{X}$ comprised of a 100×100 grid) for GP-MLE and K-EB are so similar in Figure 13. A surface for K-NLS is not shown because of the stark similarity with K-EB. Unfortunately, we do not know the real response(s) on this predictive grid, so an out-of-sample analysis must be
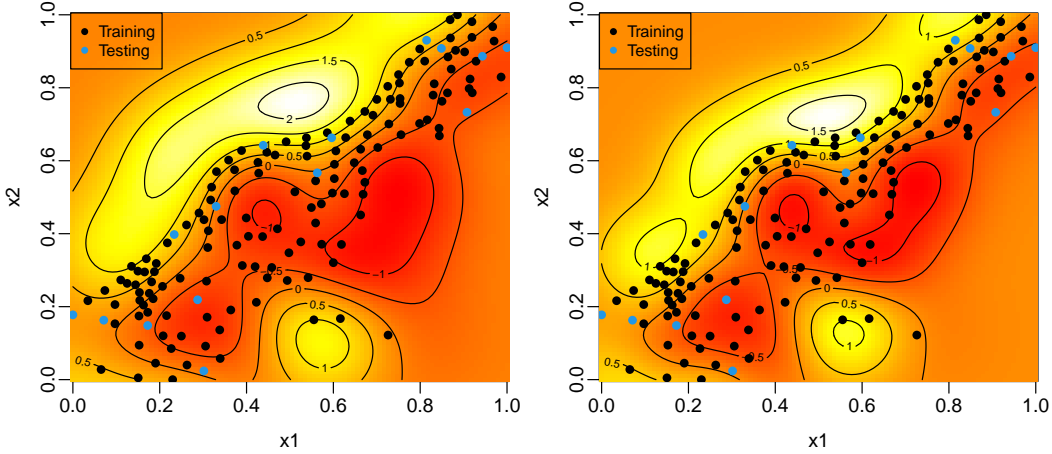
Figure 13: GP-MLE (left) and K-EB (right) predictions of log zinc.

Meuse	GP	K-EB	K-NLS
RMSE	0.103	0.109	0.108
score_f	16.79	15.97	16.50

Table 2: RMSE and score for GP and kriging on the Meuse river data on a set of 15 hold out points.

more limited than our first example. As a pre-cursor to the cross-validation scheme introduced in Section 4, we consider a simple random 90:10 train–test partition of our original 155 training data records. This results in $N = 140$ values (X_N, Y_N) that can be used for training our three models, and $N' = 15$ values $(\mathcal{X}, Y(\mathcal{X}))$ quarantined away for testing to see which works best out-of-sample by RMSE and score (again score_f from Eq.(11)). Observe that in this case there is no distinction between "true" and random y-values as we only have the testing outputs from the data. In Figure 13, the random partition is indicated by coloring the 15 testing dots blue as opposed to black. Table 2 records these values. Notice that while GPs edge out both kriging methods, the results are comparable for all three. Ideally we would repeat this enterprise multiple times, with novel 90:10 splits. For the MLE-GP this is easy, but for the kriging alternative it can be labor intensive if eyeballs are involved.